

# Multiple testing of local maxima for detection of peaks on the (celestial) sphere

Dan Cheng<sup>1</sup>, Valentina Cammarota<sup>2</sup>, Yabebal Fantaye<sup>2</sup>, Domenico Marinucci<sup>2</sup>, and  
Armin Schwartzman<sup>1</sup>

<sup>1</sup>Division of Biostatistics, University of California, San Diego

<sup>2</sup>Department of Mathematics, University of Rome Tor Vergata

March 1, 2016

## Abstract

We present a topological multiple testing scheme for detecting peaks on the sphere under isotropic Gaussian noise, where tests are performed at local maxima of the observed field filtered by the spherical needlet transform. Our setting is different from the standard Euclidean/large sample asymptotic framework, yet highly relevant to realistic experimental circumstances for some important areas of application in astronomy. More precisely, we focus on cases where a single realization of a smooth isotropic Gaussian random field on the sphere is observed, and a number of well-localized signals are superimposed on such background field. The proposed algorithms, combined with the Benjamini-Hochberg procedure for thresholding p-values, provide asymptotic strong control of the False Discovery Rate (FDR) and power consistency as the signal strength and the frequency of the needlet transform get large. This novel multiple testing method is illustrated in a simulation of point-source detection in Cosmic Microwave Background radiation (CMB) data.

- **Keywords and Phrases:** Gaussian random fields; Sphere; CMB; Height distribution; Overshoot distribution; Needlet transform; P-value; Threshold; False discovery rate; Power.
- **AMS Classification:** 60G15; 60G60; 62H15; 62M15; 62M40

## 1 Introduction

A classical problem of modern high-dimensional statistics is multiple testing in the presence of background noise. Applications are common in the areas of neuroimaging, genomic arrays and astronomy. These issues become particularly challenging when the background noise is allowed to exhibit more realistic properties than the simple *i.i.d.* framework, in particular when noise

is modeled as a stochastic process or a random field. In this setting, important progresses have been recently obtained combining ideas from two different streams of research, namely techniques from the multiple testing literature, such as False Discovery Rate (FDR) algorithms, and techniques to investigate excursion probabilities and local maxima for random fields; we refer for instance to [1, 43, 9, 10] for further background and discussion. These works have covered applications in a univariate and multivariate Euclidean setting; analytic properties have been derived under a large sample asymptotic framework, i.e., under the assumption that the domain of observations is growing steadily, together with the signals to be detected.

In this paper we introduce a related multiple testing procedure in a setting that is different from the standard Euclidean/large sample asymptotic framework, yet highly relevant to realistic experimental circumstances for some important areas of application in astronomy. More precisely, we shall focus on cases where a single realization of a smooth isotropic Gaussian random field on the sphere is observed, and a number of well-localized signals are superimposed on such background field. This is exactly the setting for the so-called point-source detection issue in Cosmic Microwave Background radiation (CMB) data experiments (see i.e., [33, 35, 34, 37]). As discussed now in any modern textbook in Cosmology (see for instance [13, 15]), CMB data can be viewed as a single realization of an isotropic Gaussian random field, which represents a “snapshot” of the Universe at the *last scattering surface*, i.e. the time (approximately  $4 \times 10^5$  years after the Big Bang, or  $1.38 \times 10^{10}$  years ago) when photons decoupled from electrons and protons and started to travel nearly without interactions in space. As such, CMB has been repeatedly defined as a goldmine of information on Cosmology - two very successful satellite experiments (WMAP from NASA, see <http://map.gsfc.nasa.gov/> and Planck from ESA, see [http://www.esa.int/Our\\_Activities/Space\\_Science/Planck](http://www.esa.int/Our_Activities/Space_Science/Planck)) have now produced full-sky maps of CMB radiations, and these data have been used in several thousand papers over the last few years to address a number of fundamental questions on the dynamics of the Big Bang, the matter-energy content of the Universe, the mechanisms of structure formation, and several others.

From the experimental point of view, it is very important to recall that, superimposed to CMB radiation, a number of foreground “contaminants” are present; as a first approximation, we can view them as point-like objects (galaxies or clusters of galaxies, typically). A major statistical challenge in the analysis of CMB data is the proper identification of such sources; on the one hand this is important for the proper construction of filtered CMB maps, on the other hand these sources are of great interest on their own as proper astrophysical objects (in some cases they can be matched with existing catalogues, while in other cases they lead to new discoveries). A number of algorithms have been proposed for these tasks, see for instance [2, 3, 25, 41, 42]. These solutions have all been shown to perform well in practice; however, they have all avoided to face the specific challenges of multiple testing, and in particular none of them has been shown to control in any proper statistical way any aggregate statistics such as the classical Family-Wise Error Rate (FWER), False Discovery Proportion (FDP) or False

Discovery Rate (FDR).

Our purpose in this paper is to develop in such a spherical framework a rigorous statistical procedure to control error rates in a multiple testing framework. Our starting idea is to extend to these circumstances the Smoothing and TESting of Maxima (STEM) algorithm advocated in [43, 10], and investigate rigorously its statistical properties. While our construction follows in several ways what was earlier done by these authors, we wish to stress that the new spherical framework poses some major technical and foundational new challenges.

The first of these new challenges is the proper definition of filters and point-like signals in a spherical framework. Here, natural solutions can be found by exploiting recent developments in the analysis of spherical random fields and spherical wavelets. In particular, we can define bell-shaped signals by adopting a natural definition of a Gaussian distribution on the sphere, motivated in terms of diffusion processes; likewise, filtering can be implemented by wavelet techniques - we find particularly convenient the Mexican needlet construction introduced by [16, 17], see also [40] for some earlier applications to CMB data.

A second, more delicate, issue is the rigorous investigation of asymptotic statistical properties. A crucial staple of the STEM algorithm is the possibility to control the FDR, assuming convergence of the empirical distribution of the maxima to its theoretical counterpart. In standard settings this can be done by resorting to ergodicity properties in a “large sample asymptotics” framework, i.e. assuming that the domain of the observations grows larger and larger. This form of ergodic properties cannot be exploited here because our spherical domain is compact. We shall hence require a convergence result on the empirical distribution of maxima in a high-frequency/fixed domain setting: this result extends to the case of the needlet transform some related computations which were recently performed in [8] for the case of random spherical harmonics. In this sense, our setting is related to the increasingly popular fixed-domain asymptotics approach for the analysis of random fields, see i.e., [23, 24].

The plan of this paper is as follows. Our basic setting and model is introduced in Section 2, with Section 3 devoted to a careful discussion on the nature and effects of filtering. Section 4 provides a description of the multiple testing scheme and discusses the error and power definitions, including the derivation of asymptotic  $p$ -values and our adoption of Benjamini and Hochberg’s (1995) pioneering approach [6]. The proofs of FDR control and tests consistency are collected in Section 5, while in Section 6 we provide some numerical results on the empirical performance of the proposed procedures in simulated CMB fields. Finally, two (long) Appendixes provide a large part of the proofs, in particular, the details of the high frequency ergodicity of the empirical distribution function of local maxima.

For clarity of exposition and concreteness of motivations, throughout the paper we mainly justify our framework resorting to applications in a Cosmological framework; it is to be stressed, however, that our approach may be applied to many other experimental contexts where data are collected on a sphere, such as Geophysics, Atmospheric Sciences, Solar Physics, and even (with some approximations) Neuroimaging, to mention only a few.

## 1.1 Acknowledgements

This research was supported by the ERC Grant n.277742 *Pascal* (PI Domenico Marinucci); we are grateful to Igor Wigman for many insights and suggestions on the computation of variances of critical points. Corresponding author: Valentina Cammarota, Department of Mathematics, University of Rome Tor Vergata, via della Ricerca Scientifica, 1, I-00133, Italy, cammarot@mat.uniroma2.it.

## 2 The model

The purpose of this Section is to introduce our model in detail. As motivated above, our purpose here is to represent a situation where a large number of “point sources” is superimposed on some isotropic background “noise”. Of course, the notions of “noise” and “signal”, here as in any other motivating field, is very much conventional. For instance, in the CMB-related applications that we have in mind the background Gaussian field is eventually the primary object of physical interest for many (most) researchers, while the super-imposed point sources are contaminants to be removed; in other astrophysical areas, on the contrary, the identification of the sources may be by itself a major scientific goal (a very recent catalogue of detected point sources/astrophysical objects is given for instance by [37]).

### 2.1 Signal model

To introduce our model for the signal, we first need to justify the notion of a “Gaussian-shaped” density on the sphere. We do this in terms of the diffusion equation on the sphere. More formally, let  $\mathbb{S}^2$  denote the unit sphere in  $\mathbb{R}^3$ . The diffusion equation on the sphere is then given by

$$\begin{aligned}\frac{\partial}{\partial t}h(x; t, x_0) &= -\Delta_{S^2} h(x; t, x_0) \\ h(x; 0, x_0) &= \delta_{x_0}(x),\end{aligned}$$

where  $\Delta_{S^2}$  is the Laplacian operator in  $\mathbb{S}^2$  and  $\delta_{x_0}(x)$  identifies formally a Dirac’s delta function centered at  $x_0 \in S^2$ . It is standard to write the solution in terms of diffusion operators as

$$h(x; t, x_0) = \exp(-t\Delta_{S^2})h(x; 0, x_0) = \sum_{\ell} \frac{2\ell + 1}{4\pi} \exp(-t\lambda_{\ell})P_{\ell}(\langle x_0, x \rangle),$$

where  $\lambda_{\ell} := \ell(\ell + 1)$  denotes the set of eigenvalues of the spherical Laplacian,  $\ell = 1, 2, \dots$ , while  $\{P_{\ell}(\cdot)\}$  represents the family of Legendre polynomials

$$P_{\ell}(u) = \frac{(-1)^{\ell}}{2^{\ell}} \frac{d^{\ell}}{du^{\ell}}(1 - u^2)^{\ell}, \quad \ell = 1, 2, 3, \dots$$

i.e.,  $P_1(u) = u$ ,  $P_2(u) = (3u^2 - 1)/2$ ,  $P_3(u) = (5u^3 - 3u)/2$ , etc., and  $\langle \cdot, \cdot \rangle$  denotes inner product on  $\mathbb{S}^2$ . By a straightforward analogy with the Euclidean case, it is natural/customary to view  $u_{x_0}(\cdot, t)$  as the density on  $\mathbb{S}^2$  of a “spherical Gaussian” centred on  $x_0$  and having variance  $t$ .

Our “point source” signal will be built from a set of such bell-shaped distributions, localized on some family of points  $\xi_k$ ,  $k = 1, \dots, N$ , belonging to  $\mathbb{S}^2$ ; we shall allow later their number to grow ( $N = N(j) \rightarrow \infty$  as  $j \rightarrow \infty$ , where  $j$  is the frequency), and their shape to become more and more localized ( $t = t_{N(j)} \rightarrow 0$  as  $N(j) \rightarrow \infty$ ). These conditions can be understood by an analogy with the (now standard) high-dimensional asymptotics framework where the number of parameters is allowed to grow to infinity in the presence of growing number of observations; likewise, we consider a growing number of sharper and sharper sources as the resolution of our experiments grow better and better, or equivalently as the scales that we are able to probe become smaller and smaller. It should be noted that, in the absence of these conditions, all our procedures to follow have properties that can be trivially established: in particular, the power of our detection procedures is very easily seen to converge to unity. More explicitly, we believe that our setting is meaningful and relevant as a guidance for applied scientists; indeed, in many circumstances (such as the CMB data analysis framework that we mentioned several times) the number of tests to implemented (i.e., the number of possible galactic sources) is in the order of several thousands, so it seems more useful to consider this quantity as diverging to infinity together with the number of observations.

## 2.2 Signal plus noise model

We can hence introduce the following sequence of signal-plus-noise models, for  $N = 1, 2, \dots$

$$y_N(x) = \mu_N(x) + z(x), \quad x \in \mathbb{S}^2, \quad (2.1)$$

where the  $\mu_N(x)$  denotes a sequence of deterministic functions on the sphere defined by

$$\mu_N(x) = \sum_{k=1}^N a_k h(x; t_N, \xi_k), \quad a_k > 0, \quad (2.2)$$

and  $h(x; t_N, \xi_k)$  is the family of “spherical Gaussian distributions” on  $\mathbb{S}^2$  (centred on  $\xi_k$  and with variance  $t_N$ ) which we introduced above by means of the heat kernel on  $\mathbb{S}^2$ , i.e.,

$$h(x; t_N, \xi_k) = \sum_{\ell=0}^{\infty} \exp(-\ell(\ell+1)t_N) \frac{2\ell+1}{4\pi} P_{\ell}(\langle \xi_k, x \rangle).$$

As mentioned earlier, we will set  $t_N \rightarrow 0$  as  $N \rightarrow \infty$ , so that each kernel  $h(x; t_N, \xi_k)$  will become in the limit more and more concentrated around its center  $\{\xi_k\}$ .

Let us now focus on the “noise” component  $z(x)$ ; here, we need to recall briefly a few standard facts on the harmonic representations of isotropic, finite variance spherical random fields. In particular, let us assume that  $\{z(x), x \in \mathbb{S}^2\}$  is Gaussian, zero-mean and isotropic, meaning that the probability laws of  $z(\cdot)$  and  $z^g(\cdot) := z(g\cdot)$  are the same for any rotation  $g \in SO(3)$ . For such fields, it is well-known that the following representation holds in the mean square sense (see for instance [22], [26]):

$$z(x) = \sum_{\ell=1}^{\infty} z_{\ell}(x), \quad z_{\ell}(x) = \sum_{m=-\ell}^{\ell} a_{\ell m} Y_{\ell m}(x), \quad (2.3)$$

where  $\{Y_{\ell m}(\cdot)\}$  denotes the family of spherical harmonics (see for instance [26], Chapters 3 and 5), and  $\{a_{\ell m}\}$  denotes the array of random spherical harmonic coefficients, which satisfy

$$a_{\ell m} = \int_{\mathbb{S}^2} z(x) \overline{Y_{\ell m}(x)} dx \quad (2.4)$$

$$\mathbb{E} a_{\ell m} \overline{a_{\ell' m'}} = C_\ell \delta_\ell^{\ell'} \delta_m^{m'}; \quad (2.5)$$

here,  $\delta_a^b$  is the Kronecker delta function, and the sequence  $\{C_\ell\}$  represents the so-called angular power spectrum of the field. As pointed out in [27], under isotropy and finite-variance the sequence  $C_\ell$  necessarily satisfies  $\sum_\ell C_\ell \frac{(2\ell+1)}{4\pi} = \mathbb{E}[z^2(x)] < \infty$  and the random field  $z(x)$  is mean square continuous. Its covariance function is given by

$$\Gamma(x_1, x_2) = \mathbb{E}[z(x_1)z(x_2)] = \sum_{\ell=0}^{\infty} \frac{2\ell+1}{4\pi} C_\ell P_\ell(\langle x_1, x_2 \rangle), \quad x_1, x_2 \in \mathbb{S}^2.$$

The Fourier components  $\{z_\ell(x)\}$ , can be viewed as random eigenfunctions of the spherical Laplacian:

$$\Delta_{\mathbb{S}^2} z_\ell = -\ell(\ell+1)z_\ell, \quad \ell = 1, 2, \dots;$$

the asymptotic behaviour of  $z_\ell(x)$  and their nonlinear transforms has been studied for instance by [44], [45] and [29].

### 3 Filtering and smoothing

An important step in the implementation of the STEM algorithm is kernel smoothing of the observed data. Given the very delicate nature of the asymptotic results in our setting, the definition of the kernel function requires here special care. We shall propose here to adopt a kernel which is based upon the so-called Mexican needlet construction introduced by [16, 18], see also [21, 30, 40] for the investigation of stochastic properties and statistical applications of these techniques.

Mexican needlets can be viewed as a natural development of the standard needlet frame which was introduced by [31, 32]. Loosely speaking, Mexican needlets differ from the standard needlet construction inasmuch as they allow for providing a kernel which is unboundedly supported in the harmonic domain; they can hence be shown to enjoy better localization properties in the real domain, i.e., faster (Gaussian rather than nearly exponential) decay of their tails. For our purposes, these better localization properties in the real domain turn out to be very important, as they allow a tight control of leakage in the signals.

The Mexican needlet transform of order  $p \in \mathbb{N}$  can be defined by

$$\Psi_j(\langle x_1, x_2 \rangle) := \sum_{\ell=0}^{\infty} b\left(\frac{\ell}{B^j}; p\right) \frac{2\ell+1}{4\pi} P_\ell(\langle x_1, x_2 \rangle); \quad (3.1)$$

here, the function  $b(\cdot; p)$  is defined by  $b(u; p) = u^{2p} e^{-u^2}$ , with  $u \in \mathbb{R}_+$ , and it is easily seen to belong to the Schwartz class (i.e., all its derivatives decay faster than any polynomial). The

user-chosen integer parameter  $p$  can be taken for simplicity to be equal to unity for all the developments that follow; more generally, it has been shown that higher values of  $p$  entail better properties in the harmonic domain, but worse real-space localization: in particular, a higher number of sidelobes (see for instance [40] for discussion and numerical evidence on these issues).

Let us now recall the standard addition theorem for spherical harmonics (see [26], eq. 3.42)

$$\sum_{m=-\ell}^{\ell} Y_{\ell m}(x_1) \bar{Y}_{\ell m}(x_2) = \frac{2\ell+1}{4\pi} P_{\ell}(\langle x_1, x_2 \rangle);$$

it is then easy to see that the “filtered noise” is given by

$$\begin{aligned} \beta_j(x) &:= \langle \Psi_j(\langle x, y \rangle), z(y) \rangle_{L^2(\mathbb{S}^2)} \\ &= \int_{\mathbb{S}^2} \sum_{\ell=0}^{\infty} b\left(\frac{\ell}{B^j}; p\right) \frac{2\ell+1}{4\pi} P_{\ell}(\langle x, y \rangle) z(y) dy \\ &= \int_{\mathbb{S}^2} \sum_{\ell=0}^{\infty} b\left(\frac{\ell}{B^j}; p\right) \sum_{m=-\ell}^{\ell} Y_{\ell m}(x) \bar{Y}_{\ell m}(y) z(y) dy \\ &= \sum_{\ell=0}^{\infty} b\left(\frac{\ell}{B^j}; p\right) \sum_{m=-\ell}^{\ell} a_{\ell m} Y_{\ell m}(x) = \sum_{\ell=0}^{\infty} b\left(\frac{\ell}{B^j}; p\right) z_{\ell}(x), \end{aligned} \tag{3.2}$$

where the last line is due to (2.3). On the other hand, for the “filtered signal” we obtain

$$\begin{aligned} \mu_{N,j}(x) &:= \sum_{k=1}^N a_k \langle \Psi_j(\langle x, y \rangle), h(y; t_N, \xi_k) \rangle_{L^2(\mathbb{S}^2)} \\ &= \sum_{k=1}^N a_k \int_{\mathbb{S}^2} \sum_{\ell=0}^{\infty} b\left(\frac{\ell}{B^j}; p\right) \frac{2\ell+1}{4\pi} P_{\ell}(\langle x, y \rangle) h(y; t_N, \xi_k) dy \\ &= \sum_{k=1}^N \sum_{\ell=0}^{\infty} a_k b\left(\frac{\ell}{B^j}; p\right) \exp(-\ell(\ell+1)t_N) \frac{2\ell+1}{4\pi} P_{\ell}(\langle \xi_k, x \rangle). \end{aligned} \tag{3.3}$$

In words, both the filtered noise and signals are averaged versions, in the harmonic domain, of (random and deterministic, respectively) Fourier components. Summing up, our kernel transform produces the sequence of smoothed fields

$$y_{N,j}(x) := \mu_{N,j}(x) + \beta_j(x), \tag{3.4}$$

Our asymptotic theory will be developed in the so-called “high-frequency” framework; more precisely, we shall introduce the following assumptions.

**Condition 1** *We have that, as  $j \rightarrow \infty$*

$$\frac{t_N}{B^{2j}} = \frac{t_N(j)}{B^{2j}} \rightarrow 0 .$$

In words, we are assuming that both the filter and the signal become more and more localized, the former more rapidly to make identification meaningful. Before we discuss these assumptions, however, we need to explore in greater detail the properties of these two components; this task is implemented in the next two subsections.

### 3.1 The filtered signal

For the analysis of the signal component  $\{\mu_{N,j}(\cdot)\}$ , it is convenient to introduce the simple approximation

$$\begin{aligned} \mu_{N,j}(x) &:= \sum_{k=1}^N \sum_{\ell=0}^{\infty} a_k \left(\frac{\ell}{B^j}\right)^{2p} \exp(-\ell(\ell+1)t_N - B^{-2j}\ell^2) \frac{2\ell+1}{4\pi} P_{\ell}(\langle \xi_k, x \rangle) \\ &= \sum_{k=1}^N \sum_{\ell=0}^{\infty} a_k \left(\frac{\ell}{B^j}\right)^{2p} \exp(-B^{-2j}\ell^2) \frac{2\ell+1}{4\pi} P_{\ell}(\langle \xi_k, x \rangle) + o_j(1) \\ &= \sum_{k=1}^N a_k \Psi_j(\langle x, \xi_k \rangle) + o_j(1), \end{aligned} \tag{3.5}$$

where the second line can be easily justified resorting to Condition 1 above. It is also known that the smoothing kernel  $\Psi_j(\langle \cdot, \xi_k \rangle)$ , for any  $\xi_k \in \mathbb{S}^2$ , has Gaussian tails (up to a polynomial factor), and hence decays faster than exponentially; more precisely one has that there exists a constant  $C_p$  such that ([16], [17], [18])

$$|\Psi_j(\langle x, \xi_k \rangle)| \leq C_p B^{2j} e^{-\frac{B^{2j} d^2(x, \xi_k)}{4}} (1 + |H_{2p}(B^j d(x, \xi_k))|), \tag{3.6}$$

where  $d(x, y) = \arccos(\langle x, y \rangle)$  is the standard geodesic distance on the sphere and  $H_q(\cdot)$  denotes the Hermite polynomial of degree  $q$ , which is defined by

$$H_q(x) = (-1)^q e^{x^2/2} \frac{d^q}{dx^q} \left( e^{-x^2/2} \right),$$

the first few being  $H_1(x) = x$ ,  $H_2(x) = x^2 - 1$ ,  $H_3(x) = x^3 - 3x, \dots$  It is also possible to provide a useful analytic approximation for the functional form of the needlet filter at the highest frequencies  $j$ ; indeed Geller and Mayeli (2009) [16] proved the following.

**Lemma 3.1** *Let  $p = 1$  and let  $\xi_k \in \mathbb{S}^2$  be fixed. Then as  $j \rightarrow \infty$ ,*

$$\Psi_j(\langle x, \xi_k \rangle) = g(d(x, \xi_k))(1 + O(B^{-2j})),$$

where

$$g(\theta) = \frac{1}{4\pi} B^{2j} e^{-\frac{B^{2j}\theta^2}{4}} \left( 1 - \frac{B^{2j}\theta^2}{4} \right), \quad \theta \in [0, \pi]$$

and  $d$  is the standard geodesic distance on the sphere.



As a consequence, we have the following analytic expression for our signal when  $p = 1$ , as  $j \rightarrow \infty$ :

$$\mu_{N,j}(x) = \sum_{k=1}^N a_k \frac{1}{4\pi} B^{2j} e^{-\frac{B^{2j} d^2(x, \xi_k)}{4}} \left( 1 - \frac{B^{2j} d^2(x, \xi_k)}{4} \right) (1 + O(B^{-2j})). \quad (3.7)$$

It is readily verified that the function  $g(\cdot)$  has the global maximum  $g(0) = \frac{1}{4\pi} B^{2j}$  and a local minimum  $g(2\sqrt{2}B^{-j}) = -\frac{1}{4\pi} e^{-2} B^{2j}$ .

### 3.2 The filtered noise

Our next step is to focus on the sequence of filtered noise fields; as derived above (equation 3.2), they can be expressed as averaged forms of random spherical eigenfunctions, e.g.

$$\beta_j(x) = \sum_{\ell=1}^{\infty} b\left(\frac{\ell}{B^j}; p\right) z_{\ell}(x), \quad j = 1, 2, 3, \dots, \quad b(u; p) = u^{2p} e^{-u^2}, \quad u \in \mathbb{R}.$$

It is convenient to normalize these fields to have unit variance, as follows:

$$\tilde{\beta}_j(x) = \frac{\beta_j(x)}{\sqrt{\mathbb{E}[\beta_{j,p}^2(x)]}}, \quad j = 1, 2, 3, \dots \quad (3.8)$$

Let us define also

$$\tilde{y}_{N,j} = \frac{y_{N,j}}{\sqrt{\mathbb{E}[\beta_{j,p}^2(x)]}} = \tilde{\beta}_j + \frac{\mu_{N,j}}{\sqrt{\mathbb{E}[\beta_{j,p}^2(x)]}}. \quad (3.9)$$

A rigorous investigation of the asymptotic properties of these smoothed fields requires some mild regularity assumptions on the power spectrum  $C_{\ell}$ , which are customary in this branch of literature. More precisely (see for instance [26], page 257 or [4, 28, 21, 30]),

**Condition 2** *There exists  $M \in \mathbb{N}, \gamma > 2$  and a function  $G(\cdot) \in C^{\infty}$  such that*

$$C_{\ell} = \ell^{-\gamma} G(\ell) \quad (3.10)$$

where  $0 < G(\ell)$  for all  $\ell$ , and for some  $c_1, \dots, c_M > 0$  and  $r = 1, \dots, M$ , we have

$$\sup_u \left| \frac{d^r}{du^r} G(u) \right| \leq c_r u^{-r}.$$

Condition 2 entails a weak smoothness requirement on the behaviour of the angular power spectrum, which is satisfied by cosmologically relevant models; for instance, this condition is fulfilled by models of the form (3.10), where  $G(\ell) = P(\ell)/Q(\ell)$  and  $P(\ell), Q(\ell) > 0$  are two positive polynomials of the same order. In what follows we denote by  $G_0$  the limit  $G_0 := \lim_{\ell \rightarrow \infty} G(\ell)$ .

Under condition 2, it is possible to establish an upper bound on the correlation function of  $\{\tilde{\beta}_j(\cdot)\}$ , as follows (for a proof see [21], [30]).

**Proposition 3.2** *Assume Conditions 2 holds with  $\gamma < 4p + 2$  and  $M \geq 4p + 2 - \gamma$ ; then there exists a constant  $K_M > 0$ , not depending on  $j$ ,  $x$ , and  $y$ , such that the following inequality holds*

$$|\text{Cor}(\tilde{\beta}_j(x), \tilde{\beta}_j(y))| \leq \frac{K_M}{(1 + j^{-1}B^j d(x, y))^{4p+2-\gamma}}, \quad (3.11)$$

where  $d(x, y) = \arccos(\langle x, y \rangle)$  is the standard geodesic distance on the sphere.

The inequality (3.11) is qualitatively similar to others which were earlier established in the case of standard needlets; see for instance [4]. A quick comparison with the results in [4] shows an important difference, namely that the rate of decay for the bound on the right-hand side depends on the shape of the kernel (in particular, on the parameter  $p$ ) and on the rate of decay of the angular power spectrum (i.e., on the parameter  $\gamma$ ); none of these values affect the rate of convergence in the standard needlet case. As a consequence, in the case of Mexican needlets, asymptotic uncorrelation only holds under the assumption that  $\gamma < 4p + 2$ , so that higher values of  $p$  are needed to ensure uncorrelation for larger values of  $\gamma$ . We believe this issue can be easily addressed by a plug-in procedure; for instance, for the CMB applications we mentioned earlier there are strong theoretical motivations and experimental constraints that allow to set  $2 < \gamma < 3$ , so that taking  $p = 1$  is already enough to ensure the correlation function decays to zero: ample numerical evidence on the uncorrelation properties of Mexican needlets is collected in [40]. The term  $j^{-1}$  appearing in the denominator of (3.11) is a consequence of some standard technical difficulties when dealing with boundary cases such as  $M = 4p + 2 - \gamma$ .

Of course, from Proposition 3.2 it is immediate to obtain a bound on the covariance (rather than correlation) function, indeed we have

$$\begin{aligned} \Gamma_{j,p}(x, y) &:= \mathbb{E}[\beta_j(x)\beta_j(y)] = \sum_{\ell=1}^{\infty} b^2\left(\frac{\ell}{B^j}; p\right) C_\ell \frac{2\ell+1}{4\pi} P_\ell(\langle x, y \rangle) \\ &\leq \frac{K_M}{(1 + j^{-1}B^j d(x, y))^{4p+2-\gamma}} \sum_{\ell=1}^{\infty} b^2\left(\frac{\ell}{B^j}; p\right) C_\ell \frac{2\ell+1}{4\pi}. \end{aligned}$$

For the implementation of our multiple testing procedures, we shall need to write down an analytic formula for the asymptotic distribution of maxima of the noise components; to this aim, we need the exact limiting behaviour of higher-order derivatives of the covariance function, evaluated at the origin. Let us first introduce the functions

$$c_{p,2n}(\gamma) := 2^{\gamma/2-2-n-2p} \Gamma(1 - \gamma/2 + n + 2p), \quad \Gamma(t) := \int_0^\infty x^{t-1} \exp(-x) dx.$$

For an isotropic Gaussian field  $\{X(x), x \in \mathbb{S}^2\}$  with covariance function

$$C(x, y) = \sum_{\ell=1}^{\infty} \frac{2\ell+1}{4\pi} C_\ell P_\ell(\langle x, y \rangle),$$

we define

$$C'(X) := \sum_{\ell=1}^{\infty} \frac{2\ell+1}{4\pi} C_\ell P'_\ell(1), \quad C''(X) := \sum_{\ell=1}^{\infty} \frac{2\ell+1}{4\pi} C_\ell P''_\ell(1),$$

where

$$P'_\ell(1) = \frac{\ell(\ell+1)}{2} \quad \text{and} \quad P''_\ell(1) = \frac{\ell(\ell-1)(\ell+1)(\ell+2)}{8}$$

represent the derivatives of the Legendre polynomials evaluated at 1. Let us write also

$$\kappa_{1,j} = \frac{C'(\tilde{\beta}_j)}{C''(\tilde{\beta}_j)}, \quad \kappa_{2,j} = \frac{[C'(\tilde{\beta}_j)]^2}{C'''(\tilde{\beta}_j)}. \quad (3.12)$$

**Proposition 3.3** *As  $j \rightarrow \infty$ , we have*

$$C'(\tilde{\beta}_j) \sim \frac{c_{p,2}(\gamma)}{2c_{p,0}(\gamma)} B^{2j}, \quad C''(\tilde{\beta}_j) \sim \frac{c_{p,4}(\gamma)}{8c_{p,0}(\gamma)} B^{4j},$$

and therefore

$$\kappa_{1,j} \sim \frac{4c_{p,2}(\gamma)}{c_{p,4}(\gamma)} B^{-2j}, \quad \kappa_{2,j} \sim \frac{2c_{p,2}^2(\gamma)}{c_{p,0}(\gamma)c_{p,4}(\gamma)};$$

where  $a_j \sim b_j$  denotes  $\lim_{j \rightarrow \infty} a_j/b_j = 1$ .

We note that the expressions for  $\kappa_{1,j}$  and  $\kappa_{2,j}$  will be used in the applied sections below for the numerical evaluation of  $p$ -values.

**Proof** Following the notation in [9], we have

$$C'(\tilde{\beta}_j) = \frac{1}{\text{Var}(\beta_j)} \sum_{\ell=0}^{\infty} b^2 \left( \frac{\ell}{B^j}; p \right) C_\ell \frac{2\ell+1}{4\pi} P'_\ell(1) = \frac{1}{\text{Var}(\beta_j)} \sum_{\ell=0}^{\infty} b^2 \left( \frac{\ell}{B^j}; p \right) C_\ell \frac{2\ell+1}{4\pi} \frac{\ell(\ell-1)}{2}$$

and

$$\begin{aligned} C''(\tilde{\beta}_j) &= \frac{1}{\text{Var}(\beta_j)} \sum_{\ell=0}^{\infty} b^2 \left( \frac{\ell}{B^j}; p \right) C_\ell \frac{2\ell+1}{4\pi} P''_\ell(1) \\ &= \frac{1}{\text{Var}(\beta_j)} \sum_{\ell=0}^{\infty} b^2 \left( \frac{\ell}{B^j}; p \right) C_\ell \frac{2\ell+1}{4\pi} \frac{\ell(\ell-1)(\ell+1)(\ell+2)}{8}. \end{aligned}$$

Indeed

$$P''_\ell(1) = \frac{\ell(\ell-1)(\ell+1)(\ell+2)}{8} = \frac{\ell(\ell+1)[\ell(\ell+1)-2]}{8} = \frac{\ell^2(\ell+1)^2}{8} - \frac{\ell(\ell+1)}{4}.$$

It is also convenient to introduce the notation

$$\begin{aligned} \mathcal{B}_{2n} = \mathcal{B}_{2n,p,j} &= \frac{1}{\sum_{\ell=1}^{\infty} b_p^2 \left( \frac{\ell}{B^j} \right) C_\ell \frac{2\ell+1}{4\pi}} \sum_{\ell=1}^{\infty} b^2 \left( \frac{\ell}{B^j}; p \right) C_\ell \frac{2\ell+1}{4\pi} \ell^n (\ell+1)^n \\ &= \frac{1}{\sum_{\ell=1}^{\infty} b_p^2 \left( \frac{\ell}{B^j} \right) \ell^{-\gamma} G(\ell) \frac{2\ell+1}{4\pi}} \sum_{\ell=1}^{\infty} b^2 \left( \frac{\ell}{B^j}; p \right) \ell^{-\gamma} G(\ell) \frac{2\ell+1}{4\pi} \ell^n (\ell+1)^n, \quad (3.13) \end{aligned}$$

for which we have

$$\begin{aligned}
\lim_{j \rightarrow \infty} B^{j(\gamma-2)} \sum_{\ell=1}^{\infty} b^2\left(\frac{\ell}{B^j}; p\right) \ell^{-\gamma} G(\ell) \frac{2\ell+1}{4\pi} &= \lim_{j \rightarrow \infty} B^{j(\gamma-2)} B^j \sum_{\ell=1}^{\infty} \int_{\frac{\ell}{B^j}}^{\frac{\ell+1}{B^j}} dx b^2\left(\frac{\ell}{B^j}; p\right) \ell^{-\gamma} G(\ell) \frac{2\ell+1}{4\pi} \\
&= \lim_{j \rightarrow \infty} B^{j(\gamma-2)} B^j \sum_{\ell=1}^{\infty} \int_{\frac{\ell}{B^j}}^{\frac{\ell+1}{B^j}} dx b^2\left(\frac{\lfloor B^j x \rfloor}{B^j}; p\right) \lfloor B^j x \rfloor^{-\gamma} G(\lfloor B^j x \rfloor) \frac{2\lfloor B^j x \rfloor + 1}{4\pi} \\
&= \lim_{j \rightarrow \infty} B^{j(\gamma-2)} B^j \int_{\frac{1}{B^j}}^{\infty} b^2\left(\frac{\lfloor B^j x \rfloor}{B^j}; p\right) \lfloor B^j x \rfloor^{-\gamma} G(\lfloor B^j x \rfloor) \frac{2\lfloor B^j x \rfloor + 1}{4\pi} dx \\
&= \lim_{j \rightarrow \infty} \int_{\frac{1}{B^j}}^{\infty} b^2\left(\frac{\lfloor B^j x \rfloor}{B^j}; p\right) \left(\frac{\lfloor B^j x \rfloor}{B^j}\right)^{-\gamma} \frac{G(\lfloor B^j x \rfloor)}{2\pi} \frac{2\lfloor B^j x \rfloor + 1}{B^j 2} dx \\
&= \frac{G_0}{2\pi} \int_0^{\infty} b^2(x; p) x^{1-\gamma} dx = \frac{G_0}{2\pi} 2^{\gamma/2-2-2p} \Gamma(1 - \gamma/2 + 2p) = c_{p,0}(\gamma).
\end{aligned}$$

Likewise

$$\begin{aligned}
c_{p,2n}(\gamma) &= \lim_{j \rightarrow \infty} B^{j(\gamma-2-2n)} \sum_{\ell=1}^{\infty} b^2\left(\frac{\ell}{B^j}; p\right) \ell^{-\gamma} G(\ell) \frac{2\ell+1}{4\pi} \ell^n (\ell+1)^n \\
&= \lim_{j \rightarrow \infty} B^{j(\gamma-2-2n)} B^j \int_{\frac{1}{B^j}}^{\infty} b^2\left(\frac{\lfloor B^j x \rfloor}{B^j}; p\right) \lfloor B^j x \rfloor^{-\gamma} G(\lfloor B^j x \rfloor) \frac{2\lfloor B^j x \rfloor + 1}{4\pi} \lfloor B^j x \rfloor^n (\lfloor B^j x \rfloor + 1)^n dx \\
&= \lim_{j \rightarrow \infty} \int_{\frac{1}{B^j}}^{\infty} b^2\left(\frac{\lfloor B^j x \rfloor}{B^j}; p\right) \left(\frac{\lfloor B^j x \rfloor}{B^j}\right)^{-\gamma} \frac{G(\lfloor B^j x \rfloor)}{2\pi} \frac{2\lfloor B^j x \rfloor + 1}{B^j 2} \left(\frac{\lfloor B^j x \rfloor}{B^j}\right)^n \left(\frac{\lfloor B^j x \rfloor + 1}{B^j}\right)^n dx \\
&= \frac{G_0}{2\pi} \int_0^{\infty} b^2(x; p) x^{2n+1-\gamma} dx = \frac{G_0}{2\pi} 2^{\gamma/2-2-n-2p} \Gamma(1 - \gamma/2 + n + 2p).
\end{aligned}$$

Hence

$$\begin{aligned}
\lim_{j \rightarrow \infty} \mathcal{B}_{2n,p,j} &= \lim_{j \rightarrow \infty} \frac{B^{j(\gamma-2)}}{B^{j(\gamma-2)} \sum_{\ell=1}^{\infty} b^2\left(\frac{\ell}{B^j}; p\right) C_{\ell} \frac{2\ell+1}{4\pi}} \frac{B^{j(\gamma-2-2n)} \sum_{\ell=1}^{\infty} b^2\left(\frac{\ell}{B^j}; p\right) C_{\ell} \frac{2\ell+1}{4\pi} \ell^n (\ell+1)^n}{B^{j(\gamma-2-2n)}} \\
&= \lim_{j \rightarrow \infty} \frac{B^{j(\gamma-2)}}{c_{p,0}(\gamma)} \frac{c_{p,2n}(\gamma)}{B^{j(\gamma-2-2n)}} = \lim_{j \rightarrow \infty} \frac{1}{c_{p,0}(\gamma)} \frac{c_{p,2n}(\gamma)}{B^{-2jn}} = \lim_{j \rightarrow \infty} \frac{c_{p,2n}(\gamma)}{c_{p,0}(\gamma)} B^{2jn}
\end{aligned}$$

and finally

$$\lim_{j \rightarrow \infty} B^{-2nj} \mathcal{B}_{2n,p,j} = \frac{c_{p,2n}(\gamma)}{c_{p,0}(\gamma)} = \frac{2^{\gamma/2-2-n-2p} \Gamma(1 - \gamma/2 + n + 2p)}{2^{\gamma/2-2-2p} \Gamma(1 - \gamma/2 + 2p)} = 2^{-n} \frac{\Gamma(1 - \gamma/2 + n + 2p)}{\Gamma(1 - \gamma/2 + 2p)}. \quad (3.14)$$

It follows that

$$\text{Var}(\beta_j) \sim \frac{c_{p,0}(\gamma)}{B^{j(\gamma-2)}}, \quad (3.15)$$

and

$$\lim_{j \rightarrow \infty} B^{-2j} C'(\tilde{\beta}_j) = \frac{\int_0^{\infty} b^2(u; p) u^{3-\gamma} du}{2 \int_0^{\infty} b^2(u; p) u^{1-\gamma} du} = \frac{c_{p,2}(\gamma)}{2c_{p,0}(\gamma)}, \quad \lim_{j \rightarrow \infty} B^{-4j} C''(\tilde{\beta}_j) = \frac{\int_0^{\infty} b^2(u; p) u^{5-\gamma} du}{8 \int_0^{\infty} b^2(u; p) u^{1-\gamma} du} = \frac{c_{p,4}(\gamma)}{8c_{p,0}(\gamma)},$$

yielding the desired results.  $\square$

In the sequel, we let  $p = 1$ ; all the results below can be trivially extended to choices of other forms of filtering, with different values of  $p$  (we stress that the case  $p = 1$  is the choice that has been usually adopted for applications, see [41, 42, 40]).

## 4 The multiple testing scheme

### 4.1 The signal and null regions

To properly approach the detection of point sources as a multiple testing problem, we first need to carefully define the spatial region occupied by the needlet-transformed point sources.

We recall that in Condition 1 we required that  $t_N \rightarrow 0$  as  $j \rightarrow \infty$ , meaning that we work in a setting where signals get more and more concentrated in the asymptotic limit; this is clearly a necessary condition for meaningful results, as we are going to handle an increasing number of signals (and tests) and, because we are working on a compact domain, in the absence of such increasing localization the problem would become entirely trivial (the signal region would cover the sphere). At the same time, we required the kernel to concentrate as well, again to avoid an excessive leakage of signal which would make the whole approach meaningless.

To be more precise, define the *signal region*  $\mathbb{D}_1^\rho = \cup_{k=1}^N D_k^\rho = \cup_{k=1}^N B(\xi_k, \rho)$  and *null region*  $\mathbb{D}_0^\rho = \mathbb{S}^2 \setminus \mathbb{D}_1^\rho$ , where  $\rho > 0$  is a pre-specified location tolerance parameter and  $D_k^\rho = B(\xi_k, \rho)$  is the geodesic ball on  $\mathbb{S}^2$  with center  $\xi_k$  and radius  $\rho$ . The presence of a tolerance parameter is not only required to settle properly the theoretical framework, but is also consistent with the common scientific practice, see again [41], [42]. We introduce now a further condition.

**Condition 3** *As  $j \rightarrow \infty$ , we have*

$$\begin{aligned} \rho = \rho_j &\sim j^\nu B^{-j} \\ \forall N, \min_{1 \leq k \neq k' \leq N} d(\xi_k, \xi_{k'}) &> \rho, \\ \inf_N \inf_{1 \leq k \leq N} a_k &> a_0, \end{aligned}$$

where  $\nu$  and  $a_0$  are positive constants.

The first two lines of Condition 3 are meant to ensure that the tolerance radius  $\rho$  decays to zero asymptotically faster than the distance between separate sources. Otherwise proper identification and counting of point sources would become unfeasible.

Notice that the restriction  $\min_{1 \leq k \neq k' \leq N} d(\xi_k, \xi_{k'}) > \rho$  in Condition 3 yields

$$\limsup_{j \rightarrow \infty} \text{Area}(B(\xi_1, \rho_j)) N_j < 4\pi = \text{Area}(\mathbb{S}^2),$$

implying that the area of null region is always positive and that  $N_j$  cannot grow too fast, specifically  $N_j = O(\rho_j^{-2}) = O(j^{-2\nu} B^{2j})$ . It is easy to check that

$$\text{Area}(B(\xi_1, \rho_j)) = 2\pi(1 - \cos \rho_j) \sim \pi \rho_j^2 \sim \pi j^{2\nu} B^{-2j}.$$

Here are some examples for Condition 3. If  $N_j = B^{2j(1-\delta)}$  for some  $0 < \delta < 1/2$ , then the area of signal region tends to 0. If  $N_j = c_0 \rho_j^{-2} = c_0 j^{-2\nu} B^{2j}$  for some  $c_0 \in (0, 4)$ , then the area of signal region tends to  $\pi c_0$ .

## 4.2 The STEM algorithm on the sphere

As some general notation, for a smooth Gaussian random field  $\{X(x), x \in \mathbb{S}^2\}$ , define the number of local maxima of  $X$  exceeding the level  $u \in \mathbb{R}$  over a domain  $D \subset \mathbb{S}^2$  as

$$M_u(X; D) = \# \{x \in D : X(x) > u, \nabla X(x) = 0, \nabla^2 X(x) \prec 0\}; \quad (4.1)$$

here  $\nabla X(x)$  and  $\nabla^2 X(x)$  denote the gradient and Hessian of the field  $X$  at  $x$ , and  $\nabla^2 X(x) \prec 0$  means the Hessian  $\nabla^2 X(x)$  is negative definite. The gradient and Hessian can be computed as  $\nabla X = (E_1 X, E_2 X)$  and  $\nabla^2 X = (E_i E_j X)_{1 \leq i, j \leq 2}$ , respectively, where  $E_1$  and  $E_2$  are orthonormal tangent vectors. In spherical coordinates  $0 \leq \theta \leq \pi$ ,  $0 \leq \varphi < 2\pi$ , these are given by

$$E_1 = \frac{\partial}{\partial \theta}, \quad E_2 = \frac{1}{\sin \theta} \frac{\partial}{\partial \varphi}.$$

For convenience, denote by  $M(X; D) = M_{-\infty}(X; D)$  the total number of local maxima of  $X$  over  $D$ .

Suppose now we observe  $y_N(t)$  on  $\mathbb{S}^2$  defined by (2.1). The STEM algorithm of [43, 10] takes in our case the following form.

### Algorithm 1 (STEM algorithm)

1. Kernel smoothing: *Apply the needlet transform to the observed field (2.1) to obtain the filtered field (3.4). Normalize by the (known) noise variance to obtain the field (3.9).*
2. Candidate peaks: *Find the set of local maxima of  $y_{N,j}(x)$  on  $\mathbb{S}^2$*

$$\tilde{T}_{N,j} = \{x \in \mathbb{S}^2 : \nabla \tilde{y}_{N,j}(x) = 0, \nabla^2 \tilde{y}_{N,j}(x) \prec 0\}. \quad (4.2)$$

3. P-values: *For each  $x \in \tilde{T}_{N,j}$ , compute the p-value  $p_{N,j}(x)$  for testing*

$$\begin{aligned} \mathcal{H}_0(x) &: \{\mu_{N,j}(y) = 0 \text{ for all } y \in B(x, \rho_j)\} \quad \text{vs.} \\ \mathcal{H}_A(x) &: \{\mu_{N,j}(y) > 0 \text{ for some } y \in B(x, \rho_j)\} \end{aligned} \quad (4.3)$$

where  $B(x, \rho_j)$  is a geodesic ball centered at  $x$  on the sphere and of radius equal to the tolerance radius  $\rho_j$ .

4. Multiple testing: *Notice that  $M(\tilde{y}_{N,j}; \mathbb{S}^2) = \#\{x \in \tilde{T}_{N,j}\}$  is the number of tested hypotheses. Perform a multiple testing procedure on the set of  $M(\tilde{y}_{N,j}; \mathbb{S}^2)$  p-values  $\{p_{N,j}(x), x \in \tilde{T}_{N,j}\}$ , and declare significant all local maxima whose p-values are smaller than the significance threshold.*

Next, we carefully define detection errors and power for this testing scheme.

### 4.3 Error and power definitions

Now, for fixed  $u \in \mathbb{R}$ , denote by  $\tilde{T}_{N,j}(u)$  the set of local maxima exceeding  $u$  defined via (4.1). Define the total number of detected peaks and the number of falsely detected peaks as

$$R_j(u) = M_u(\tilde{y}_{N,j}; \mathbb{S}^2), \quad V_{\rho_j}(u) = M_u(\tilde{y}_{N,j}; \mathbb{D}_0^{\rho_j}), \quad (4.4)$$

respectively. Both are defined as zero if  $\tilde{T}_{N,j}(u)$  is empty. As usual, the False Discovery Proportion (FDP) is proportion of falsely detected peaks, i.e.

$$\text{FDP}_{\rho_j}(u) = \frac{V_{\rho_j}(u)}{R_j(u) \vee 1} = \frac{M_u(\tilde{y}_{N,j}; \mathbb{D}_0^{\rho_j})}{M_u(\tilde{y}_{N,j}; \mathbb{D}_0^{\rho_j}) + M_u(\tilde{y}_{N,j}; \mathbb{D}_1^{\rho_j})}, \quad (4.5)$$

while the False Discovery Rate (FDR) is the expected FDP, i.e.

$$\text{FDR}_{\rho_j}(u) = \mathbb{E} \left\{ \frac{V_{\rho_j}(u)}{R_j(u) \vee 1} \right\}. \quad (4.6)$$

We shall denote  $W_{\rho_j}(u) = R_j(u) - V_{\rho_j}(u)$ .

Finally, again following the same conventions as in [43], [10], we define the power of Algorithm 1 as the expected fraction of true discovered peaks

$$\text{Power}_{\rho_j}(u) = \mathbb{E} \left( \frac{1}{N_j} \sum_{k=1}^{N_j} \mathbb{1}_{\{\tilde{T}_{N,j}(u) \cap D_k^{\rho_j} \neq \emptyset\}} \right) = \frac{1}{N_j} \sum_{k=1}^{N_j} \text{Power}_{\rho_j,k}(u), \quad (4.7)$$

where  $\text{Power}_{\rho_j,k}(u)$  is the probability of detecting peak  $k$

$$\text{Power}_{\rho_j,k}(u) = \mathbb{P} \left( \tilde{T}_{N,j}(u) \cap D_k^{\rho_j} \neq \emptyset \right). \quad (4.8)$$

The indicator function in (4.7) ensures that only one significant local maximum is counted within the same peak support, so power is not inflated.

### 4.4 P-values and BH algorithm

Given the observed heights  $y_{N,j}(x)$  at the local maxima  $x \in \tilde{T}_{N,j}$ , the p-values in step (3) of Algorithm 1 are computed as  $p_{N,j}(t) = F_j(y_{N,j}(t))$ ,  $t \in \tilde{T}_{N,j}$ , where

$$F_j(u) = \mathbb{P} \left( \tilde{\beta}_j(x) > u \mid x \in \tilde{T}_{N,j} \right) \quad (4.9)$$

denotes the right tail probability of  $\tilde{\beta}_j(x)$  at the local maximum  $x \in \tilde{T}_{N,j}$ , evaluated under the complete null hypothesis  $\mu(x) = 0, \forall x$ .

Applying the technique of [11], we have that

$$F_j(u) = \frac{\mathbb{E}[M_u(\tilde{\beta}_j; \mathbb{S}^2)]}{\mathbb{E}[M(\tilde{\beta}_j; \mathbb{S}^2)]} = \int_u^\infty f_j(x) dx, \quad (4.10)$$

where

$$f_j(x) = \frac{2\sqrt{3 + \kappa_{1,j}}}{2 + \kappa_{1,j}\sqrt{3 + \kappa_{1,j}}} \left\{ [\kappa_{1,j} + \kappa_{2,j}(x^2 - 1)] \phi(x) \Phi \left( \frac{\sqrt{\kappa_{2,j}}x}{\sqrt{2 + \kappa_{1,j} - \kappa_{2,j}}} \right) + \frac{\sqrt{\kappa_{2,j}(2 + \kappa_{1,j} - \kappa_{2,j})}}{2\pi} x e^{-\frac{(2 + \kappa_{1,j})x^2}{2(2 + \kappa_{1,j} - \kappa_{2,j})}} + \frac{\sqrt{2}}{\sqrt{\pi(3 + \kappa_{1,j} - \kappa_{2,j})}} e^{-\frac{(3 + \kappa_{1,j})x^2}{2(3 + \kappa_{1,j} - \kappa_{2,j})}} \Phi \left( \frac{\sqrt{\kappa_{2,j}}x}{\sqrt{(2 + \kappa_{1,j} - \kappa_{2,j})(3 + \kappa_{1,j} - \kappa_{2,j})}} \right) \right\}.$$

Here  $\kappa_{1,j}$ ,  $\kappa_{2,j}$  are defined in (3.12) above, and  $\phi(x)$  and  $\Phi(x)$  denote the standard normal density and distribution functions, respectively.

We can now apply the BH procedure in step (4) of Algorithm 1, as follows. For a fixed significance level  $\alpha \in (0, 1)$ , let  $k$  be the largest index for which the  $i$ th smallest  $p$ -value is less than  $i\alpha/M(\tilde{y}_{N,j}; \mathbb{S}^2)$ . Then the null hypothesis  $\mathcal{H}_0(x)$  at  $x \in \tilde{T}_{N,j}$  is rejected if

$$p_{N,j}(x) < \frac{k\alpha}{M(\tilde{y}_{N,j}; \mathbb{S}^2)} \iff \tilde{y}_{N,j}(x) > \tilde{u}_{\text{BH},j} = F_j^{-1} \left( \frac{k\alpha}{M(\tilde{y}_{N,j}; \mathbb{S}^2)} \right), \quad (4.11)$$

where  $k\alpha/M(\tilde{y}_{N,j}; \mathbb{S}^2)$  is defined as 1 if  $M(\tilde{y}_{N,j}; \mathbb{S}^2) = 0$ . Since  $\tilde{u}_{\text{BH},j}$  is random, definition (4.6) is hereby modified to

$$\text{FDR}_{\text{BH},\rho_j} = \mathbb{E} \left\{ \frac{V_{\rho_j}(\tilde{u}_{\text{BH},j})}{R_j(\tilde{u}_{\text{BH},j}) \vee 1} \right\}, \quad (4.12)$$

where  $R_j(\cdot)$  and  $V_{\rho_j}(\cdot)$  are defined in (4.4) and the expectation is taken over all possible realizations of the random threshold  $\tilde{u}_{\text{BH},j}$ .

Since  $\tilde{u}_{\text{BH},j}$  is random, similarly to the definition of  $\text{FDR}_{\text{BH},\rho}$  (4.12), we define

$$\text{Power}_{\text{BH},\rho_j} = \mathbb{E} \left( \frac{1}{N_j} \sum_{k=1}^{N_j} \mathbb{1}_{\{\tilde{T}_{N,j}(\tilde{u}_{\text{BH},j}) \cap D_k^{\rho} \neq \emptyset\}} \right). \quad (4.13)$$

## 5 FDR Control and Power Consistency

### 5.1 FDR Control

The strategy to prove FDR control is to first quantify the expected number of local maxima above any level  $u$  over the null region (false discoveries) and signal region (true discoveries). This is given in Lemmas 5.1 and 5.3 below.

**Lemma 5.1** *Let  $u \in \mathbb{R}$  be fixed. Then as  $j \rightarrow \infty$ , the expected number of local maxima of  $\tilde{y}_{N,j}$  above  $u$  in the null region  $\mathbb{D}_0^{\rho_j}$  is*

$$\mathbb{E}[M_u(\tilde{y}_{N,j}; \mathbb{D}_0^{\rho_j})] = [4\pi - 2\pi(1 - \cos \rho_j)N_j]r_j(u) + o(e^{-j^\nu}), \quad (5.1)$$

where

$$r_j(u) = \mathbb{E}[M_u(\tilde{\beta}_{N,j}; \mathbb{S}^2)] = F_j(u)r_j, \quad u \in \mathbb{R}, \quad (5.2)$$



is the expected number of local maxima of  $\tilde{\beta}_j$  exceeding  $u$  over a unit area on  $\mathbb{S}^2$ ,  $F_j(u)$  is the tail distribution function (4.10), and

$$r_j = r_j(-\infty) = \frac{1}{4\pi} + \frac{1}{2\pi\kappa_{1,j}\sqrt{3 + \kappa_{1,j}}}. \quad (5.3)$$

**Proof** Recall  $\text{Area}(B(\xi_k, \rho_j)) = 2\pi(1 - \cos \rho_j)$  for every  $k$ , therefore

$$\text{Area}(\mathbb{D}_0^{\rho_j}) = \text{Area}(\mathbb{S}^2) - \text{Area}(B(\xi_k, \rho_j))N_j = 4\pi - 2\pi(1 - \cos \rho_j)N_j.$$

By the Kac-Rice metatheorem, Lemma 3.1 and Condition 3,

$$\begin{aligned} & \mathbb{E}[M_u(\tilde{y}_{N,j}; \mathbb{D}_0^{\rho_j})] \\ &= \int_{\mathbb{D}_0^{\rho_j}} \frac{1}{2\pi\sqrt{\det\text{Cov}(\nabla\tilde{y}_{N,j}(x))}} \mathbb{E}[|\det(\nabla^2\tilde{y}_{N,j}(x))| \mathbb{1}_{\{\tilde{y}_{N,j}(x) > u, \nabla^2\tilde{y}_{N,j}(x) < 0\}} | \nabla\tilde{y}_{N,j}(x) = 0] dx \\ &= \int_{\mathbb{D}_0^{\rho_j}} \frac{1}{2\pi\sqrt{\det\text{Cov}(\nabla\tilde{\beta}_j(x))}} \mathbb{E}[|\det(\nabla^2\tilde{\beta}_j(x))| \mathbb{1}_{\{\tilde{\beta}_j(x) > u, \nabla^2\tilde{\beta}_j(x) < 0\}} | \nabla\tilde{\beta}_j(x) = 0] dx \\ &+ O(N_j B^m j^{2\nu} e^{-j^{2\nu}}), \end{aligned}$$

where  $m$  is some positive constant. Evaluating the integral yields (5.1), where

$$r_j(u) = \frac{1}{2\pi C'(\tilde{\beta}_j)} \mathbb{E}[|\det(\nabla^2\tilde{\beta}_j(x))| \mathbb{1}_{\{\tilde{\beta}_j(x) > u, \nabla^2\tilde{\beta}_j(x) < 0\}} | \nabla\tilde{\beta}_j(x) = 0]$$

is the expected number of local maxima of  $\tilde{\beta}_j$  exceeding  $u$  over a unit area on  $\mathbb{S}^2$ . The exact expression (5.2) follows from (4.10), while (5.3) was proved in [11].  $\square$

**Remark 5.2** [Asymptotics of  $r_j(u)$ .] By Proposition 3.3, as  $j \rightarrow \infty$ ,

$$\kappa_{1,j} \sim \frac{4c_{p,2}(\gamma)}{c_{p,4}(\gamma)} B^{-2j},$$

implying for (5.3) and (5.2) that

$$r_j \sim \frac{c_{p,4}(\gamma)}{8\pi\sqrt{3}c_{p,2}(\gamma)} B^{2j}, \quad r_j(u) = F_j(u)r_j \sim F_j(u) \frac{c_{p,4}(\gamma)}{8\pi\sqrt{3}c_{p,2}(\gamma)} B^{2j}.$$

**Lemma 5.3** Let  $u \in \mathbb{R}$  be fixed. Then as  $j \rightarrow \infty$ , the number of local maxima of  $\tilde{y}_{N,j}$  over the signal region  $\mathbb{D}_1^{\rho_j}$  satisfies

$$\begin{aligned} M_u(\tilde{y}_{N,j}; \mathbb{D}_1^{\rho_j}) &\geq N_j + O_p(B^{-2j}) \\ \mathbb{E}[M_u(\tilde{y}_{N,j}; \mathbb{D}_1^{\rho_j})] &\geq N_j + O(B^{-2j}). \end{aligned}$$

**Proof** Let  $\tilde{\rho}_j = B^{-j} < \rho_j = j^\nu B^{-j}$ . By Lemma 3.1, within the domain  $B(\xi_k, \tilde{\rho}_j)$ , the mean function of  $\tilde{y}_{N,j}$  satisfies the assumptions of the unimodal signal model in [10] with the signal strength being  $a = B^{2j}$ . It then follows from similar arguments as in [10] that

$$\begin{aligned} M_u(\tilde{y}_{N,j}; \mathbb{D}_1^{\tilde{\rho}_j}) &= N_j + O_p(B^{-2j}) \\ \mathbb{E}[M_u(\tilde{y}_{N,j}; \mathbb{D}_1^{\tilde{\rho}_j})] &= N_j + O(B^{-2j}). \end{aligned}$$

The desired results then follow immediately from the observation

$$M_u(\tilde{y}_{N,j}; \mathbb{D}_1^{\rho_j}) \geq M_u(\tilde{y}_{N,j}; \mathbb{D}_1^{\tilde{\rho}_j}),$$

where the inequality admits the possibility of there being other local maxima in the flatter areas  $B(\xi_k, \rho_j) \setminus B(\xi_k, \tilde{\rho}_j)$  of the needlet transform impulse response. The exact expected number of these is presumably small, but hard to estimate.  $\square$

**Remark 5.4** [The rate of  $\rho_j$ ] The proof of Lemma 5.3 explains why we make the assumption  $\rho_j \sim j^\nu B^{-j}$  in Condition 3 above. This choice of rate for  $\rho_j$ , decaying slightly less slowly than  $B^{-j}$ , allows obtaining an asymptotic limit to the number of local maxima over the null region  $\mathbb{E}[M_u(\tilde{y}_{N,j}, \mathbb{D}_0^{\rho_j})]$ , while the number of local maxima over the signal region  $\mathbb{E}[M_u(\tilde{y}_{N,j}, \mathbb{D}_1^{\rho_j})]$  can be bounded asymptotically. If we had chosen the rate of  $\tilde{\rho}_j$  for  $\rho_j$ , decaying at a rate  $B^{-j}$ , then as shown in the proof of Lemma 5.3, we could obtain an exact limit for the number of local maxima over the signal region; however in that case, the number of local maxima over the null region would be difficult to quantify due to complicated behavior of the mean function  $\tilde{\mu}_{N,j}$  (after the needlet transform) immediately outside that radius.

The following ergodic result, which will be used in the proof of Theorem 5.6 below, shows that the variance of the number of local maxima goes to zero after normalization by the expected value. The result itself is theoretically important and the proof is given in the Appendix.

**Theorem 5.5** *As  $j \rightarrow \infty$*

$$\text{Var}[M_u(\tilde{\beta}_j; \mathbb{S}^2)] \leq c(u)j^2 B^{2j} + o(j^2 B^{2j}).$$

where the constant  $c(u)$  is uniformly bounded with respect to  $u$  and the  $o(\cdot)$  term is universal.

Following is the first main result of this paper, showing control of FDP and FDR.

**Theorem 5.6** *Let the assumptions in the model and Condition 3 hold.*

(i) *Suppose that Algorithm 1 is applied with a fixed threshold  $u$ , then*

$$\text{FDP}_{\rho_j} \leq \frac{[4\pi - 2\pi(1 - \cos \rho_j)N_j]r_j(u)}{[4\pi - 2\pi(1 - \cos \rho_j)N_j]r_j(u) + N_j}(1 + o_p(1)), \quad (5.4)$$

where  $r_j(u)$  is defined in (5.2).

(ii) Suppose that Algorithm 1 is applied with the random threshold  $\tilde{u}_{\text{BH},j}$  (4.11), then

$$\text{FDR}_{\text{BH},\rho_j} \leq \alpha \frac{[4\pi - 2\pi(1 - \cos \rho_j)N_j]r_j}{[4\pi - 2\pi(1 - \cos \rho_j)N_j]r_j + N_j} + o(1), \quad (5.5)$$

where  $r_j$  is given by (5.3).

### Proof

(i) By Theorem 5.5 and Chebyshev's inequality,

$$\begin{aligned} \text{FDP}_{\rho_j}(u) &= \frac{M_u(\tilde{y}_{N,j}; \mathbb{D}_0^{\rho_j})/B^{2j}}{M_u(\tilde{y}_{N,j}; \mathbb{D}_0^{\rho_j})/B^{2j} + M_u(\tilde{y}_{N,j}; \mathbb{D}_1^{\rho_j})/B^{2j}} \\ &\leq \frac{\mathbb{E}[M_u(\tilde{y}_{N,j}; \mathbb{D}_0^{\rho_j})]/B^{2j}}{\mathbb{E}[M_u(\tilde{y}_{N,j}; \mathbb{D}_0^{\rho_j})]/B^{2j} + M_u(\tilde{y}_{N,j}; \mathbb{D}_1^{\rho_j})/B^{2j}} (1 + o_p(1)). \end{aligned}$$

It then follows from Lemmas 5.1 and 5.3 that

$$\text{FDP}_{\rho_j}(u) = \frac{[4\pi - 2\pi(1 - \cos \rho_j)N_j]r_j(u)}{[4\pi - 2\pi(1 - \cos \rho_j)N_j]r_j(u) + N_j} (1 + o_p(1)).$$

(ii) Following a similar argument to that in [10], we use the fact that  $\tilde{u}_{\text{BH},j}$  is the smallest  $u$  satisfying  $\alpha \tilde{G}_{N,j}(u) \geq F_j(u)$ , where

$$\tilde{G}_{N,j}(u) = \frac{M_u(\tilde{y}_{N,j}; \mathbb{D}_0^{\rho_j}) + M_u(\tilde{y}_{N,j}; \mathbb{D}_1^{\rho_j})}{M(\tilde{y}_{N,j}; \mathbb{D}_0^{\rho_j}) + M(\tilde{y}_{N,j}; \mathbb{D}_1^{\rho_j})}$$

and  $F_j(u)$  is the height distribution (4.10) of  $\tilde{\beta}_j$ . Notice that

$$F_j(u) = \frac{\mathbb{E}[M_u(\tilde{y}_{N,j}; \mathbb{D}_0^{\rho_j})]}{\mathbb{E}[M(\tilde{y}_{N,j}; \mathbb{D}_0^{\rho_j})]}.$$

Similarly to the proof of part (i), we have

$$\begin{aligned} \tilde{G}_{N,j}(u) &\geq \frac{\mathbb{E}[M(\tilde{y}_{N,j}; \mathbb{D}_0^{\rho_j})]F_j(u) + N_j}{\mathbb{E}[M(\tilde{y}_{N,j}; \mathbb{D}_0^{\rho_j})] + N_j} + o_p(1) \\ &= \frac{[4\pi - 2\pi(1 - \cos \rho_j)N_j]r_j F_j(u) + N_j}{[4\pi - 2\pi(1 - \cos \rho_j)N_j]r_j + N_j} + o_p(1). \end{aligned}$$

Solving the equation

$$\alpha \frac{[4\pi - 2\pi(1 - \cos \rho_j)N_j]r_j F_j(u) + N_j}{[4\pi - 2\pi(1 - \cos \rho_j)N_j]r_j + N_j} + o_p(1) = F_j(u)$$

gives an asymptotic solution

$$\tilde{u}_{\text{BH},j}^* = F_j^{-1} \left( \frac{\alpha N_j}{N_j + (1 - \alpha)[4\pi - 2\pi(1 - \cos \rho_j)N_j]r_j} \right) + o_p(1). \quad (5.6)$$

Since  $\tilde{u}_{\text{BH},j} \leq \tilde{u}_{\text{BH},j}^*$  almost surely, we have

$$\begin{aligned} \text{FDR}_{\text{BH},j} &= \mathbb{E} \left[ \frac{V_{\rho_j}(\tilde{u}_{\text{BH},j})}{V_{\rho_j}(\tilde{u}_{\text{BH},j}) + W_{\rho_j}(\tilde{u}_{\text{BH},j})} \right] \leq \mathbb{E} \left[ \frac{V_{\rho_j}(\tilde{u}_{\text{BH},j}^*)}{V_{\rho_j}(\tilde{u}_{\text{BH},j}^*) + W_{\rho_j}(\tilde{u}_{\text{BH},j}^*)} \right] \\ &\leq \frac{\mathbb{E}[V_{\rho_j}(\tilde{u}_{\text{BH},j}^*)]}{\mathbb{E}[V_{\rho_j}(\tilde{u}_{\text{BH},j}^*)] + \mathbb{E}[W_{\rho_j}(\tilde{u}_{\text{BH},j}^*)]} (1 + o(1)) \leq \frac{\mathbb{E}[M(\tilde{y}_{N,j}; \mathbb{D}_0^{\rho_j})] F_j(\tilde{u}_{\text{BH},j}^*)}{\mathbb{E}[M(\tilde{y}_{N,j}; \mathbb{D}_0^{\rho_j})] F_j(\tilde{u}_{\text{BH},j}^*) + N_j} (1 + o(1)) \\ &= \alpha \frac{[4\pi - 2\pi(1 - \cos \rho_j)N_j]r_j}{[4\pi - 2\pi(1 - \cos \rho_j)N_j]r_j + N_j} + o(1). \end{aligned}$$

□

**Remark 5.7 [Threshold for FDP]** To make FDP asymptotically equal to a significance level  $\alpha$ , the corresponding threshold  $u$  must satisfy the equation

$$\frac{[4\pi - 2\pi(1 - \cos \rho_j)N_j]r_j(u)}{[4\pi - 2\pi(1 - \cos \rho_j)N_j]r_j(u) + N_j} = \alpha,$$

implying

$$r_j(u) = \frac{\alpha N_j}{(1 - \alpha)[4\pi - 2\pi(1 - \cos \rho_j)N_j]}. \quad (5.7)$$

By Remark 5.2,

$$r_j(u) \sim F_j(u) \frac{c_{p,4}(\gamma)}{8\pi\sqrt{3}c_{p,2}(\gamma)} B^{2j},$$

implying that as  $j \rightarrow \infty$  and  $u \rightarrow \infty$ ,

$$\log(r_j(u)) \sim \log(B^{2j}e^{-u^2/2}).$$

Solving the equation

$$B^{2j}e^{-u^2/2} = \frac{\alpha N_j}{(1 - \alpha)[4\pi - 2\pi(1 - \cos \rho_j)N_j]}$$

yields the approximate solution

$$u \sim \sqrt{2 \log(B^{2j}/N_j)}. \quad (5.8)$$

According to Condition 3,  $N_j \rho_j^2 = O(1)$ , implying  $N_j = O(\rho_j^{-2}) = O(j^{-2}B^{2j})$ . Therefore,  $u \geq \sqrt{\log(j)} \rightarrow \infty$ .

**Remark 5.8 [Comparison between FDP and BH Procedure.]** Dividing both sides of (5.7) by  $r_j$  yields

$$F_j(u) = \frac{\alpha N_j}{(1 - \alpha)[4\pi - 2\pi(1 - \cos \rho_j)N_j]r_j},$$

implying the following threshold by FDP for controlling significance level  $\alpha$ :

$$u_\alpha = F_j^{-1} \left( \frac{\alpha N_j}{(1 - \alpha)[4\pi - 2\pi(1 - \cos \rho_j)N_j]r_j} \right).$$

In comparison, for controlling significance level  $\alpha$  by the BH procedure, the asymptotic threshold is given by (5.6). If we replace  $\alpha$  by

$$\tilde{\alpha} = \alpha \frac{[4\pi - 2\pi(1 - \cos \rho_j)N_j]r_j}{[4\pi - 2\pi(1 - \cos \rho_j)N_j]r_j + N_j},$$

then the FDP threshold at significance level  $\tilde{\alpha}$  is given by

$$u_{\tilde{\alpha}} = F_j^{-1} \left( \frac{\alpha N_j}{N_j + (1 - \alpha)[4\pi - 2\pi(1 - \cos \rho_j)N_j]r_j} \right).$$

This coincides with the asymptotic threshold  $\tilde{u}_{\text{BH},j}^*$  (5.6) by BH procedure. Since  $r_j = O(B^{2j})$  and  $N_j = O(\rho_j^{-2}) = O(j^{-2}B^{2j})$ , we see that the upper bound in (5.5) tends to  $\alpha$  in the limit of high-frequency.

**Remark 5.9 [Comparison with FWER control (expected Euler characteristic).]** For high values of the threshold  $u$ , the expected Euler characteristic exceeding  $u$  can be approximated by  $r_j(u)$ ; hence, the threshold for controlling the FWER can be obtained by solving the equation  $r_j(u) = \alpha$ . By the discussion in the previous remark, this equation becomes  $B^{2j}e^{-u^2/2} = \alpha$ , which gives the solution

$$u \sim \sqrt{2 \log(B^{2j})} = 2\sqrt{j \log(B)}.$$

In comparison, the FDR threshold increases at a rate  $\sqrt{\log(j)}$ , much slower.

## 5.2 Power Consistency

To prove power consistency, we first show that, asymptotically, there will be at least one local maximum of  $\tilde{y}_{N,j}$  within a small ball centered at every point source.

**Lemma 5.10** *For each fixed  $k$ , there exists  $c > 0$  such that for sufficiently large  $j$ ,*

$$\mathbb{P} \left( \#\{x \in \tilde{T}_{N,j}(u) \cap D_k^{\tilde{\rho}}\} \geq 1 \right) \geq 1 - \exp \left( -cB^{j(\gamma-2)/2} \right),$$

where  $\tilde{\rho} = B^{-j}$  and  $u = \sqrt{2 \log(B^{2j}/N_j)}$  is the asymptotic BH threshold (5.8).

**Proof** For each  $k$ , the probability  $\tilde{y}_{N,j}(x)$  has at least one local maximum above  $u$  in  $D_k^{\tilde{\rho}} = B(\xi_k, \tilde{\rho})$  is the complement of the probability that: (1)  $\tilde{y}_{N,j}(x)$  has no local maxima in  $D_k^{\tilde{\rho}}$ , or (2)  $\tilde{y}_{N,j}(x)$  is below  $u$  everywhere in  $D_k^{\tilde{\rho}}$ .

For (1), this is less than the probability that there exists some  $x \in D_k^{\rho_1}$  such that  $\langle \nabla \tilde{y}_{N,j}(x), \xi_k - x \rangle \leq 0$ , since all  $x \in \partial D_k^{\tilde{\rho}}$  satisfying  $\langle \nabla \tilde{y}_{N,j}(x), \xi_k - x \rangle > 0$  would imply the existence of at

least one local maximum in  $D_k^{\tilde{\rho}}$ . This probability is bounded above by

$$\begin{aligned} & \mathbb{P} \left( \inf_{\partial D_k^{\tilde{\rho}}} \langle \nabla \tilde{\beta}_j(x), \xi_k - x \rangle \leq - \inf_{\partial D_k^{\tilde{\rho}}} \langle \nabla \tilde{\mu}_{N,j}(x), \xi_k - x \rangle \right) \\ &= \mathbb{P} \left( \sup_{\partial D_k^{\tilde{\rho}}} - \left\langle \nabla \tilde{\beta}_j(x), \frac{\xi_k - x}{\|\xi_k - x\|} \right\rangle \geq \inf_{\partial D_k^{\tilde{\rho}}} \left\langle \nabla \tilde{\mu}_{N,j}(x), \frac{\xi_k - x}{\|\xi_k - x\|} \right\rangle \right) \\ &\leq \mathbb{P} \left( \sup_{x \in D_k^{\tilde{\rho}}} \sup_{\|\tau\|=1} \langle \nabla \tilde{\beta}_j(x), \tau \rangle \geq c_1 B^{2j+j(\gamma-2)/2} \right), \end{aligned}$$

where  $c_1$  is a positive constant and the last inequality is due to (3.15), (3.7), Lemma 3.1 and the fact that  $\partial D_k^{\tilde{\rho}}$  is contained in the closure of  $D_k^{\tilde{\rho}}$ . By Proposition 3.3, there exists  $c_2 > 0$  such that for sufficiently large  $j$ ,

$$\sup_{x \in D_k^{\tilde{\rho}}} \sup_{\|\tau\|=1} \text{Var}(\langle \nabla \tilde{\beta}_j(x), \tau \rangle) \leq c_2 B^{2j}.$$

Then by the Borell-TIS inequality, there exists  $c_3 > 0$  such that for sufficiently large  $j$ ,

$$\mathbb{P} \left( \#\{x \in \tilde{T}_{N,j} \cap D_k^{\tilde{\rho}}\} = 0 \right) \leq \exp \left( -c_3 B^{j(\gamma-2)/2} \right).$$

On the other hand, for (2), the probability that  $\tilde{y}_{N,j}(x)$  is below  $u$  everywhere in  $D_k^{\tilde{\rho}}$  is bounded above by  $1 - \Phi(|u - B^{2j+j(\gamma-2)/2}|)$ . The desired result then follows from the observation

$$\mathbb{P} \left( \#\{x \in \tilde{T}_{N,j}(u) \cap D_k^{\tilde{\rho}}\} \geq 1 \right) \geq 1 - \exp \left( -c_3 B^{j(\gamma-2)/2} \right) - \left( 1 - \Phi(|u - B^{2j+j(\gamma-2)/2}|) \right),$$

where the last term in parentheses is much smaller than the second when  $u = \sqrt{2 \log(B^{2j}/N_j)}$ .  
□

Following is the second main result of this paper, showing that the detection power tends to one asymptotically.

**Theorem 5.11** *Let the assumptions in the model and Condition 3 hold.*

(i) *Suppose that Algorithm 1 is applied with a fixed threshold  $u$ , then*

$$\text{Power}_{\rho_j}(u) \rightarrow 1.$$

(ii) *Suppose that Algorithm 1 is applied with the random threshold  $\tilde{u}_{\text{BH}}$  (4.11), then*

$$\text{Power}_{\text{BH}, \rho_j} \rightarrow 1.$$

**Proof** The desired results follow directly from Lemma 5.10 and the definitions of power (4.7) and (4.13). □

## 6 Numerical Validation

In this section we present numerical evidence on the performance of the algorithm advocated in this work. One crucial step in the STEM algorithm (Algorithm 1) is the computation of p-values of detected peaks, based on the distribution of peak heights under the complete noise assumption. We therefore start our validation by comparing the analytical peak height distribution function given in Eqn. (4.10) with the empirical result from filtered noise Monte Carlo simulations.

Once we establish the validity of the peak height distribution on the noise field, we add simulated point sources to form the full signal-plus-noise Monte Carlo simulations. These simulations are used to evaluate the numerical performance of the asymptotic FDP approximation and FDR control of Section 5.

### 6.1 Simulation of the CMB noise field

All our maps and the corresponding spherical harmonic coefficients are generated using the *HEALpix* package, which is now the standard routine software for handling cosmological data: see [19] for a detailed discussion on this package and its main features. In *HEALpix* one can use the *create\_alm* routine to generate random spherical harmonic coefficients,  $a_{\ell m}$ , with a given power spectrum. The code *alm2map* takes these coefficients and generate a pixelized Gaussian map; the inverse process is implemented using the *map2alm* code. To decompose a map into Mexican needlet components, we filter the  $a_{\ell m}$  coefficients by the Mexican needlet window functions as given in Eqn. (3.2).

A single *HEALpix* pixel has an area of  $4\pi/N_{\text{pix}}$  where  $N_{\text{pix}} = 12N_{\text{side}}^2$  is the total number of pixels on a given map. The resolution is specified by the  $N_{\text{side}}$  parameter, which is a multiple of 2.

To simulate our noise field, we generated 100 Gaussian realization maps of the CMB sky starting from the Planck CMB power spectrum. All maps are simulated with a pixel resolution of  $N_{\text{side}} = 1024$ . The standard deviation, also called root mean square (RMS), of the simulated noise field is given by

$$\sigma_{\text{noise}}^2 = \sigma_{\text{cmb}}^2 = \sum_{\ell} \frac{(2\ell + 1)C_{\ell}}{4\pi}, \quad (6.1)$$

where  $C_{\ell}$  is the Planck CMB power spectrum [36].

To simulate the finite resolution of the measuring instrument, these maps are then smoothed by a Gaussian filter with full-width half max (FWHM) of 10 arcmin. In the literature, this is usually referred to as a 10 arcmin Gaussian beam. Its effect can be thought of as part of the noise autocovariance function, although it is essentially negligible at  $\ell \sim 1000$  as in our needlet analysis.

## 6.2 Simulation of point sources

As mentioned above, a point source in the sky is observed by a detector which has a finite angular resolution. With some abuse of nomenclature, the opening angle of the smallest resolvable angular unit,  $t_N$ , is called the beam of the detector. The typical angular size of galaxies is of a few arcsecs (i.e., one degree divided by  $60^2$ ) while the detector beam sizes for typical CMB experiments (10 arcmin) are an order of magnitude larger. This means that galaxies and other objects with angular size smaller than the beam can be viewed as point sources. As argued in the previous sections, the convolution of the point sources by the detector beam yields a Gaussian bell-like profile in the final map with the peak of the Gaussian being at the location of the point sources,  $\xi_k$ . The signal part of our simulations is hence given by equation Eqn. (2.2) above, where the coefficient  $a_k$  represent the brightness of the  $k$ th point source and  $N$  is their total number.

It would be possible to consider more realistic models for these point sources, for instance using the so-called Planck sky model (see i.e., [12]). However, this would require a rather lengthy technical discussion on some specific astrophysical and experimental settings, which would not add anything substantial to the understanding of our current algorithm, nor would alter significantly our numerical results. We therefore delay a more complete analysis of these practical issues to a future, more applied paper.

To simulate our signal model with  $N$  point sources, we first generated  $N$  coordinate points randomly with a uniform probability density over the sphere. Second we found the pixels that correspond to these locations on the HEALpix map; third we set the values  $a_k$  of these pixels as draws from a uniform distribution in the range 0 and  $A_{\max}$ . These amplitudes are given as a multiple of the RMS of the noise (6.1). Finally, to simulate the instrumental resolution, we convolved the map obtained in the last step by means of a Gaussian beam of FWHM = 10 arcmin. This final map is now a pixelized version of (2.1). Notice that for clarity we have described the smoothing process as a separate operation in the noise and signal maps, but this is, of course, equivalent to doing a single smoothing operation on a signal plus noise map.

The Gaussian beam decreases the sources magnitude by a factor proportional to the ratio between the area of a pixel and the area covered by the detector beam. For our choice of the beam and the pixel resolution, this factor is an order of magnitude. Since we desired to generate point sources uniformly distributed between 0 and  $3\sigma_{noise}$  after smoothing, we used  $A_{max} = 30\sigma_{cmb}$ . We considered different values for the total number of sources, i.e.,  $N=1000, 3000, 5000$ .

The final signal-plus-noise Monte Carlo simulations are then obtained by adding the point sources map to the 100 noise simulations; an example is provided in Fig.(1). Note that the point sources are weak and hard to find without statistical analysis.



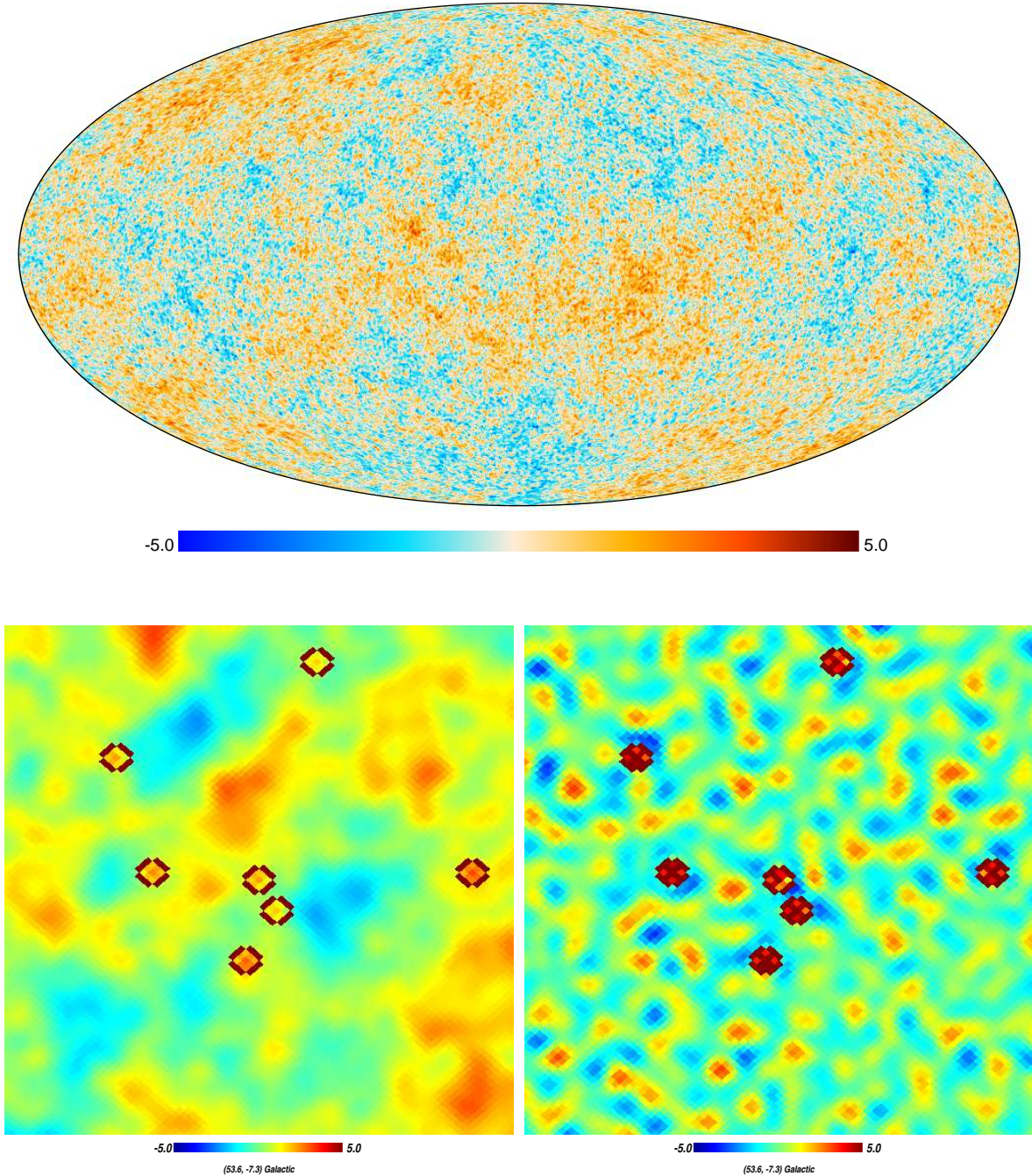


Figure 1: **Signal plus noise maps:** Upper panel is an equal area stereographic projection (the so called Mollweide projection) of the signal plus noise simulation before needlet filtering. The color map is given in standardized RMS units. Bottom left panel is a gnomonic projection of the unfiltered map around a point source with 5 degree diameter; bottom right panel is a similar gnomonic projection around the same point source but from a Mexican needlet filtered map. The Mexican needlet parameters used are  $j = 38$ ,  $B = 1.2$  and  $p = 1$ . The red marks have been added only to visualize the location of the point sources but are not part of the simulation.

### 6.3 Distribution of peak heights

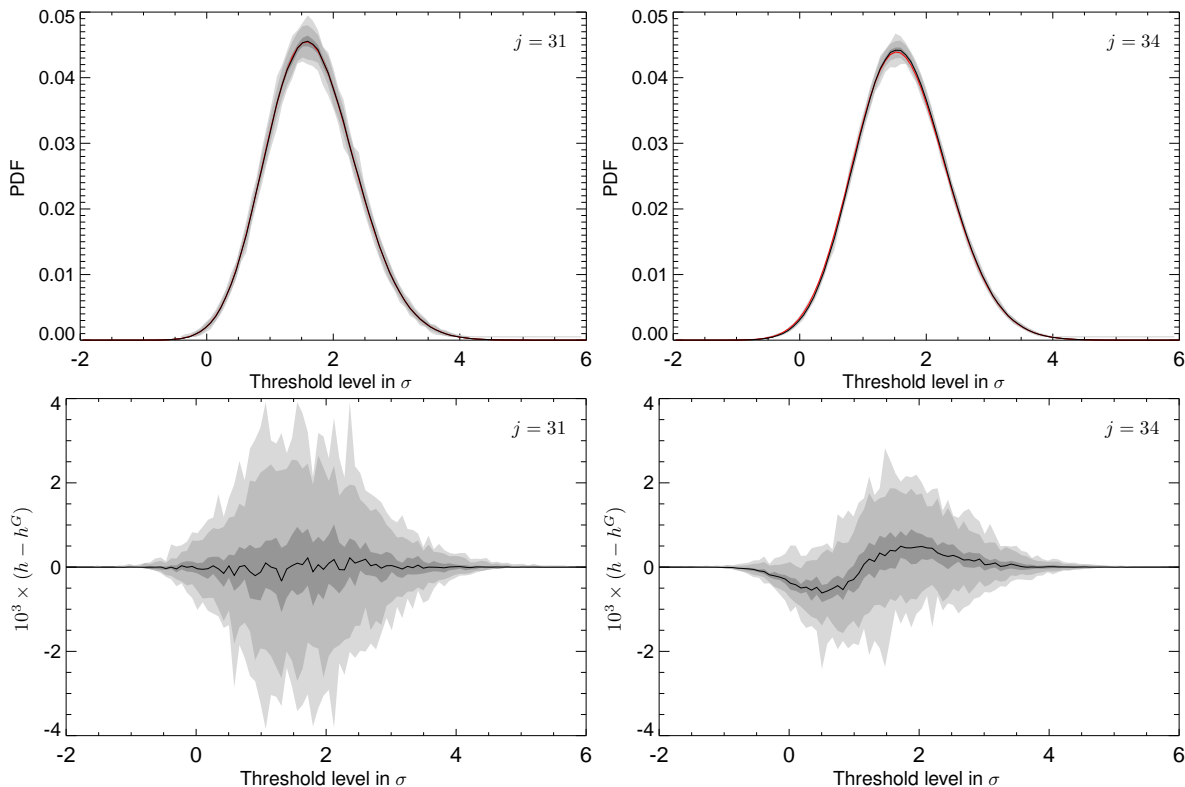


Figure 2: **Peaks PDF:** probability density of height of local maxima. In the upper panels, the red curves represent the analytical values, while the black curves and the gray contours are the mean and the 68,95,99 % percentiles from the simulations from 100 Monte Carlo simulations with no point sources. The lower panels show the difference between the analytical ( $h^G$ ) and numerical ( $h$ ) result. The mexican needlet parameters used are  $p = 1$ ,  $B = 1.2$  and  $j = 31, 34$ , which corresponds to central multipoles of  $\ell = [284, 492]$ .

The theoretical distribution of local maxima (peaks) on a Mexican needlet filtered Gaussian map is given by Eqn. (4.10). In Fig. (2) we present the comparison of the theoretical density,  $h_j(x)$ , with what we obtained empirically using 100 Gaussian map simulations with no point sources. The upper panels from left to right respectively present the normalized Gaussian peak PDFs for needlet frequency  $j = 31, 34$ , with Mexican needlet parameters  $B = 1.2$  and  $p = 1$ . We chose these values as a natural compromise which on one hand illustrates higher multipoles behaviour, on the other hand still allows for extremely good numerical accuracy (better than 1% precision for finding peaks).

In the lower panel of Fig. (2) we show the relative percentage difference between the analytical and simulation results. It is easy to see from these figures that the theory fits the numerical results remarkably well. Moreover, the dispersion around the expected value of the

PDF decreases as  $j$  increases, consistently with the ergodicity result of Theorem 5.5.

### 6.4 Application of the STEM algorithm

The first step in the STEM algorithm, after needlet filtering, is to normalize the map using its standard deviation, as defined in Eqn. (3.8), to obtain Eqn. (3.9).

To find local peaks on a map we compute the first and second derivatives using HEALpix 's routine *alm2map\_der*. The pixels where the first derivative is close to zero (within a precision of  $10^{-6}$ ) are classified as the local extrema. We then partition these extrema into maxima, minima and saddle using the eigenvalue decomposition of the Hessian matrix - of course, maxima are those with all the eigenvalues negative.

It is instructive to look at how the brightness of point sources increase as we filter the signal plus noise map with Mexican needlets. In Fig. (3), we plot the PDF of point source amplitudes before adding noise (grey curve), after adding noise but before needlet filtering (thick black curve), and after filtering with increasing  $j$ . For the high frequency Mexican needlet we considered,  $j = 38$ , filtering increases the brightness by a factor greater than 4. The negative values in the histogram are due to the added Gaussian noise; we do not expect to detect such weak sources based on their amplitude information only.

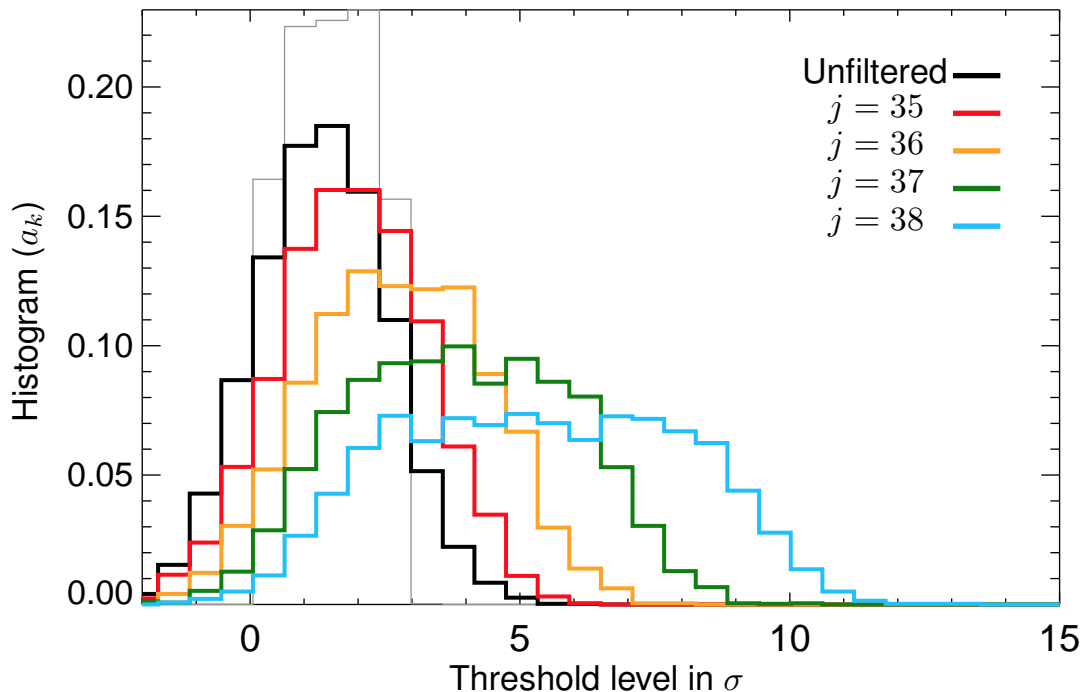


Figure 3: **Needlet filtering increases signal-to-noise ratio:** Histogram of signal amplitudes at the location of the point sources, before adding noise (grey curve), after adding noise but before filtering (thick black curve), and after filtering with the Mexican needlet at different  $j$ . The Mexican needlet parameters used are  $B = 1.2$  and  $p = 1$ .

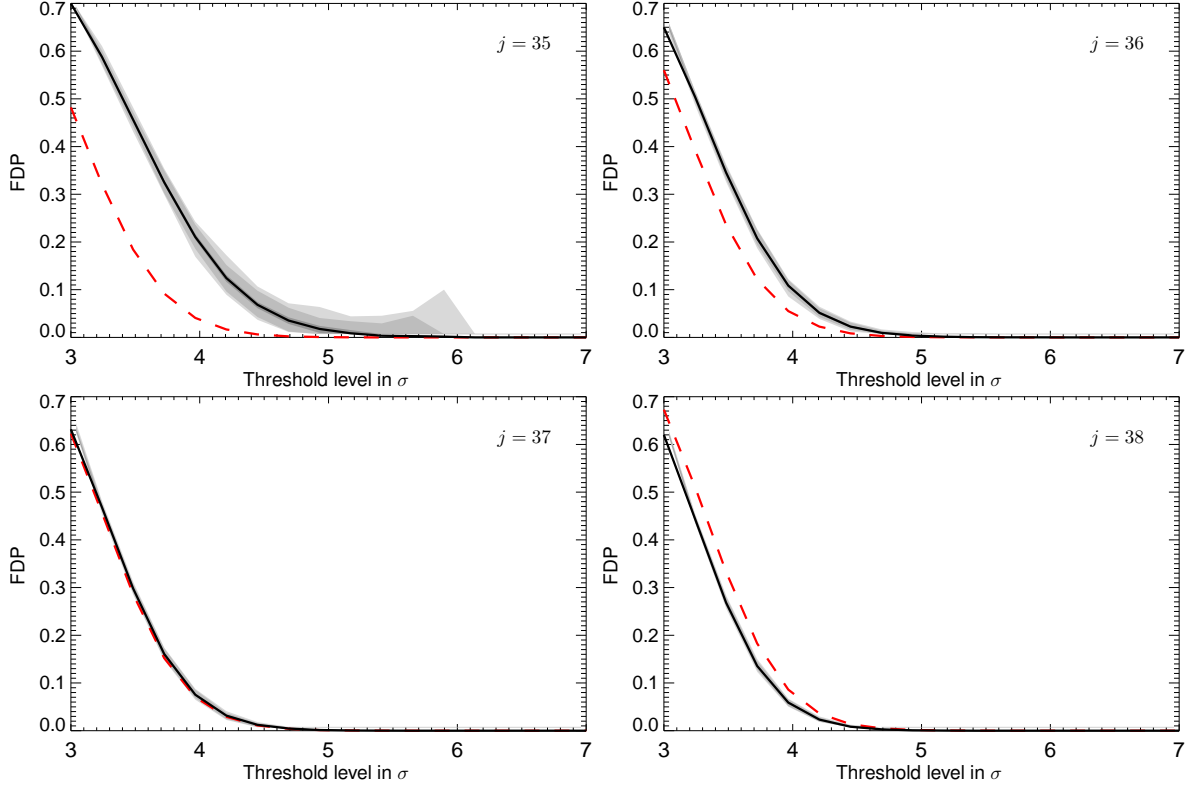


Figure 4: **False Discovery Proportion:** FDP as a function of threshold (in units of standard deviation) for different needle scales. The dashed red curves are for the analytical upper bounds while the black curves are for the mean of the empirical FDPs from 100 Monte Carlo simulations. The gray shades are for percentiles 68, 95 and 99%. The Mexican needlelet parameters used are  $B = 1.2$  and  $p = 1$ .

## 6.5 False Discovery Proportion (FDP)

In Eqn. (5.5) of Section 5 we provided the analytical result on the upper bound of the FDP as a function of the power spectrum of the noise, the total number and the spatial profile of the sources. Here we compare this result with what is obtained from numerical simulations.

The empirical FDP is computed using the following steps: locate maxima on needlelet filtered signal-plus-noise Monte Carlo simulations using our peak detection code; classify peaks as *True discovery* if the location of a maxima corresponds to a known (input) point source within  $\rho$  pixel radius or *False discovery* if there are no input sources within  $\rho$  pixels radius of the peak ( $\rho$  corresponding to the tolerance parameter); count the number of True and False discoveries as a function of  $\rho$  and the RMS of the noise.

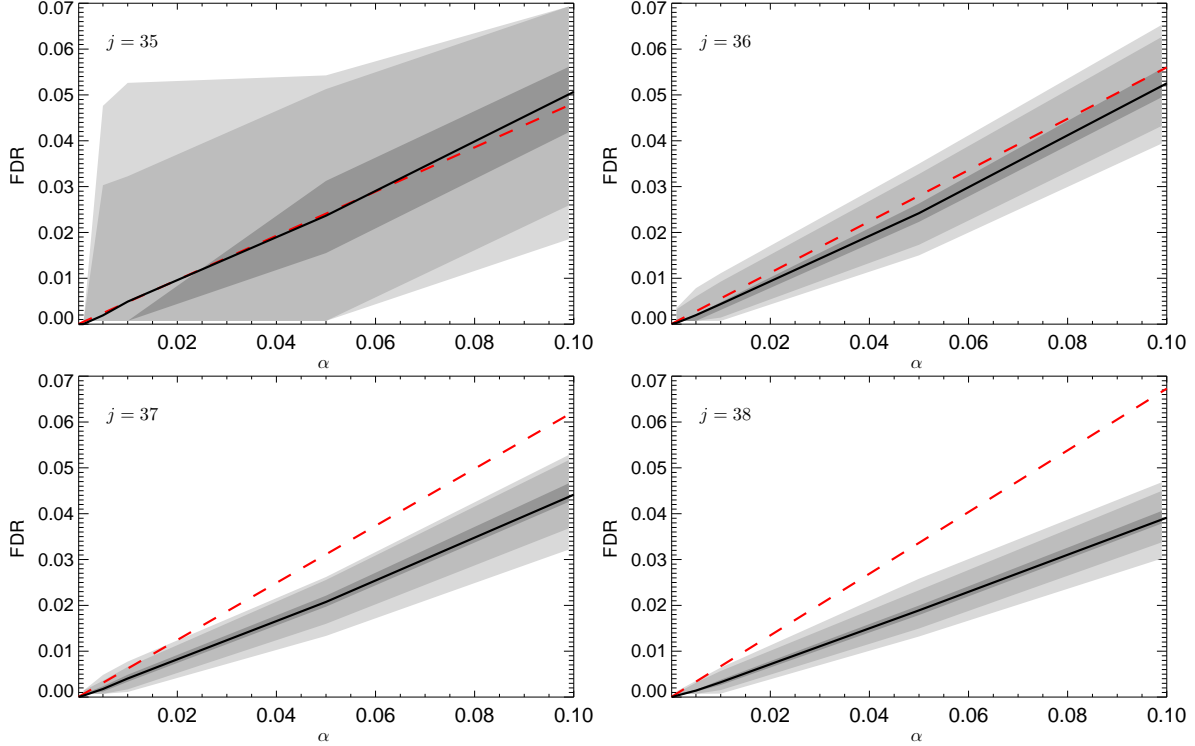


Figure 5: **False Discovery Rate:** FDR as a function of error rate  $\alpha$  for different needle scales. The red curve is a plot of  $\alpha * FDP(u = 3)$ , while the black curve is the mean from 100 Monte Carlo simulations. The gray shades are for percentiles 68, 95 and 99%. The number of point sources is 5000. The Mexican needlelet parameters used are  $B = 1.2$  and  $p = 1$ .

The empirical FDP as a function of  $u$ , which is in units of the RMS of the noise, and the source detection tolerance parameter  $\rho$  is computed, according to (4.5), as

$$\widehat{FDP}_{\rho_j}(u) = \frac{\# \text{ of False discoveries above } u}{\text{total } \# \text{ of peaks above } u} \quad (6.2)$$

In Fig. (4) we illustrate the comparison of the FDP for thresholds in the filtered map above  $3\sigma$  and  $\rho = 3$  for different values of  $j$ . We found that setting  $2 \leq \rho \leq 8$  does not alter significantly our results (note that the smallest practical radius is  $\rho = 2$ ). The red curve in these plots corresponds to the first term on the right hand side of Eqn. (5.5), while the black curve is from the mean of the simulations. The contours from dark to light gray corresponds to the 68, 95 and 99% confidence intervals. We note that, as expected, the analytic results for the upper bound become larger than the numerical simulations as  $j$  increases.



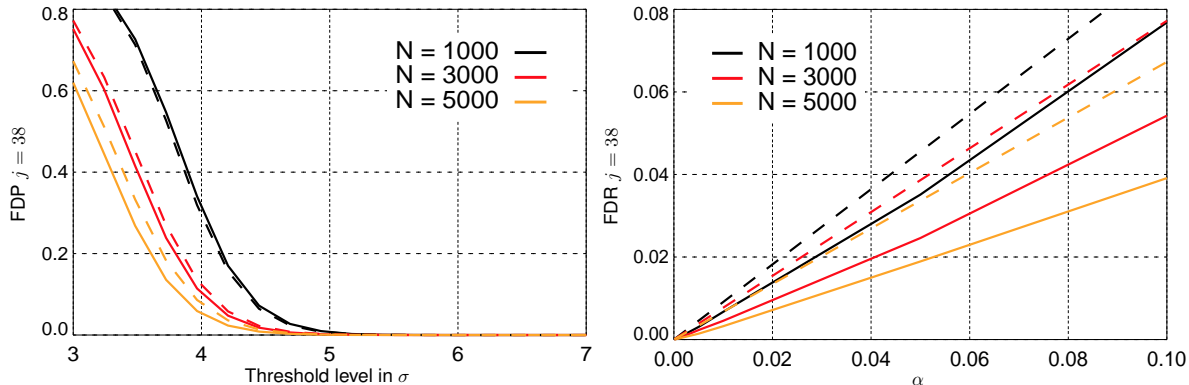


Figure 6: **Theoretical vs numerical results for FDP and FDR:** FDP as a function of thresholds and FDR as a function of global p-value,  $\alpha$ , for needlet scale  $j = 38$ . The dashed curves are the analytical upper bounds while the solid curves are the corresponding empirical results from 100 Monte Carlo simulations. The Mexican needlet parameters used are  $B = 1.2$  and  $p = 1$

## 6.6 False Discovery Rate (FDR)

We now proceed in validating the analytical formalism established in Section 5 to control the false discovery rate (FDR). This is done by comparing the analytical upper bound of the FDR, which is given by Eqn. (5.5), with the empirical result from simulations. In Fig. (5), it is shown that for a given error rate, the empirical FDR is always below the upper limit set by the theory.

In Fig. (6) we present the mean FDP and FDR curves together with the corresponding theoretical results for different number of input sources. Again, the FDP and FDR are bounded above by the theoretical bounds.

## 6.7 Detection power

To quantify how many of the input point sources we discovered in our analysis, in Fig. (7) we show the number of peaks that matches the true sources i.e., the numerator of (4.7), which measures the statistical power of the algorithm. These results show that the power of the STEM algorithm is almost 100% in detecting bright sources - indeed, we have detected all input sources whose brightness was above  $1\sigma$  in the unfiltered simulated maps.

Overall, we believe that the results in this section provide a strong numerical support for the asymptotic findings that we described earlier in this paper.

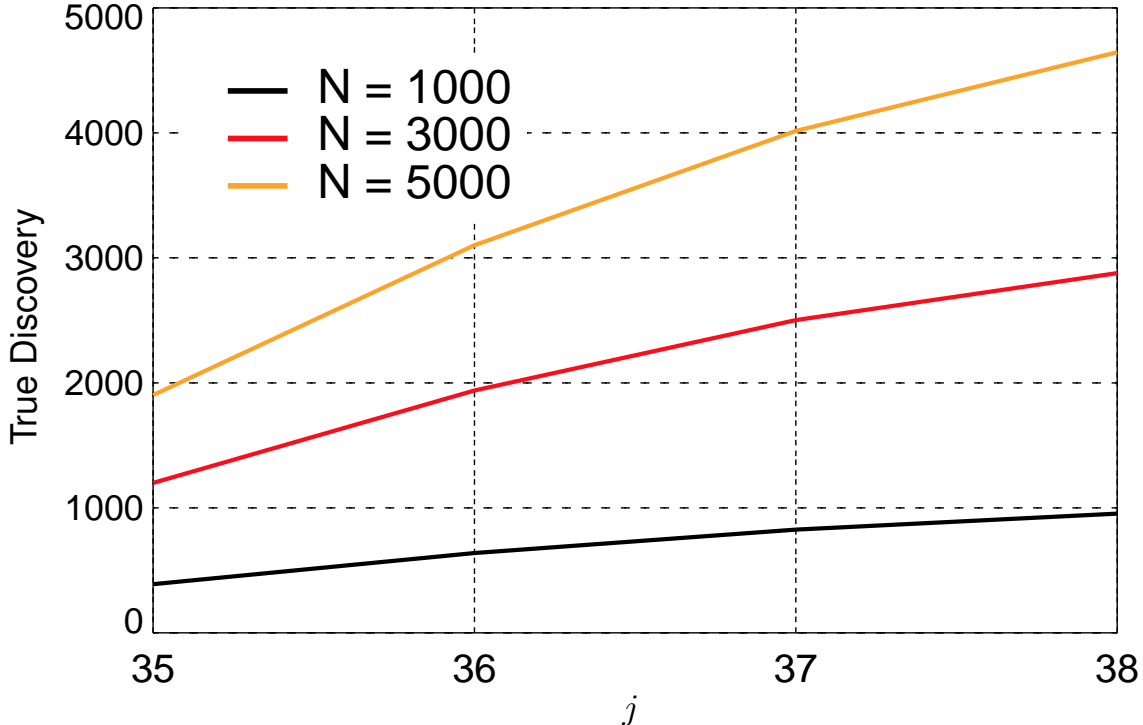


Figure 7: **Detection power:** number of true discoveries for threshold  $u > 3$  as a function of needlet scales,  $j$ . The three curves are the mean of 100 Monte Carlo simulations for the corresponding cases. The legend shows the number of input point sources in simulations. The Mexican needlet parameters used are  $B = 1.2$  and  $p = 1$ .

## A Proof of Theorem 5.5

### A.1 Voronoi cells

We introduce the following notation for the spherical caps in  $\mathbb{S}^2$ :

$$\mathcal{B}(a, \varepsilon) = \{x \subseteq \mathbb{S}^2 : d(a, x) \leq \varepsilon\}.$$

For any  $\varepsilon > 0$ , we say that  $\Xi_\varepsilon = \{\xi_{1,\varepsilon}, \dots, \xi_{N,\varepsilon}\}$  is a *maximal  $\varepsilon$ -net*, if  $\xi_{1,\varepsilon}, \dots, \xi_{N,\varepsilon}$  are in  $\mathbb{S}^2$ ,  $\forall i \neq j$  we have  $d(\xi_{i,\varepsilon}, \xi_{j,\varepsilon}) > \varepsilon$  and  $\forall x \in \mathbb{S}^2$ ,  $d(x, \Xi_\varepsilon) \leq \varepsilon$ . Heuristically, an  $\varepsilon$ -net is a grid of point at a distance at least  $\varepsilon$  from each other, and such that any extra point should be within a distance  $\varepsilon$  from a point in the grid, see [5, Lemma 5]. The number  $N$  of points in a  $\varepsilon$ -net on the sphere can be bounded from above and from below, indeed we have the following:

$$\frac{4}{\varepsilon^2} \leq N \leq \frac{4}{\varepsilon^2} \pi^2.$$

Given an  $\varepsilon$ -net it is natural to partition the sphere into disjoint sets, each of them associated with a single point in the net. This task is accomplished by the well-known Voronoi cells construction.

**Definition A.1** Let  $\Xi_\varepsilon$  be a maximal  $\varepsilon$ -net. For all  $\xi_{i,\varepsilon} \in \Xi_\varepsilon$ , the associated family of Voronoi cells is defined by

$$\mathcal{V}(\xi_{i,\varepsilon}, \varepsilon) = \{x \in \mathbb{S}^2 : \forall j \neq i, d(x, \xi_{i,\varepsilon}) \leq d(x, \xi_{j,\varepsilon})\}.$$

We recall that  $\mathcal{B}(\xi_{i,\varepsilon}, \varepsilon/2) \subseteq \mathcal{V}(\xi_{i,\varepsilon}, \varepsilon) \subseteq \mathcal{B}(\xi_{i,\varepsilon}, \varepsilon)$ , hence  $\text{Area}(\mathcal{V}(\xi_{i,\varepsilon}, \varepsilon)) \approx \varepsilon^2$ . Let

$$\mathcal{N}^c(\tilde{\beta}_j; \mathcal{V}(\xi_{i,\varepsilon}, \varepsilon), I) = \#\{x \in \mathcal{V}(\xi_{i,\varepsilon}, \varepsilon) : \tilde{\beta}_j(x) \in I, \nabla \tilde{\beta}_j(x) = 0\}.$$

Note that, almost surely, the sum of the critical points over the Voronoi cells equals the total number of critical points:

$$\mathcal{N}_I^c(\tilde{\beta}_j) = \sum_{\xi_{i,\varepsilon} \in \Xi_\varepsilon} \mathcal{N}^c(\tilde{\beta}_j; \mathcal{V}(\xi_{i,\varepsilon}, \varepsilon), I).$$

Our proof uses similar ideas to those exploited in [8] for the analysis of critical points of spherical random eigenfunctions. In particular, we split the variance into two terms, one related to the correlation between Voronoi cells which are further apart than an (asymptotically vanishing) threshold (the so-called ‘‘long-range component’’), the other related to Voronoi cells whose distance is smaller than the threshold.

More precisely, we have that

$$\begin{aligned} \text{Var} \left( \mathcal{N}_I^c(\tilde{\beta}_j) \right) &= \sum_{\xi_{i,\varepsilon}, \xi_{k,\varepsilon} \in \Xi_\varepsilon} \text{Cov} \left( \mathcal{N}^c(\tilde{\beta}_j; \mathcal{V}(\xi_{i,\varepsilon}, \varepsilon), I), \mathcal{N}^c(\tilde{\beta}_j; \mathcal{V}(\xi_{k,\varepsilon}, \varepsilon), I) \right) \\ &= \sum_{d(\mathcal{V}(\xi_{i,\varepsilon}, \varepsilon), \mathcal{V}(\xi_{k,\varepsilon}, \varepsilon)) > C/B^j} \text{Cov} \left( \mathcal{N}^c(\tilde{\beta}_j; \mathcal{V}(\xi_{i,\varepsilon}, \varepsilon), I), \mathcal{N}^c(\tilde{\beta}_j; \mathcal{V}(\xi_{k,\varepsilon}, \varepsilon), I) \right) \end{aligned} \quad (1.1)$$

$$+ \sum_{d(\mathcal{V}(\xi_{i,\varepsilon}, \varepsilon), \mathcal{V}(\xi_{k,\varepsilon}, \varepsilon)) \leq C/B^j} \text{Cov} \left( \mathcal{N}^c(\tilde{\beta}_j; \mathcal{V}(\xi_{i,\varepsilon}, \varepsilon), I), \mathcal{N}^c(\tilde{\beta}_j; \mathcal{V}(\xi_{k,\varepsilon}, \varepsilon), I) \right). \quad (1.2)$$

In Section A.2 we prove that the asymptotic behaviour of the long-range component (1.1) is

$$\sum_{d(\mathcal{V}(\xi_{i,\varepsilon}, \varepsilon), \mathcal{V}(\xi_{k,\varepsilon}, \varepsilon)) > C/B^j} \text{Cov} \left( \mathcal{N}^c(\tilde{\beta}_j; \mathcal{V}(\xi_{i,\varepsilon}, \varepsilon), I), \mathcal{N}^c(\tilde{\beta}_j; \mathcal{V}(\xi_{k,\varepsilon}, \varepsilon), I) \right) \leq c_1(I)j^2 B^{2j} + o(j^2 B^{2j}) \quad (1.3)$$

while in Section A.3 we prove that for (1.2) we have

$$\sum_{d(\mathcal{V}(\xi_{i,\varepsilon}, \varepsilon), \mathcal{V}(\xi_{k,\varepsilon}, \varepsilon)) \leq C/B^j} \text{Cov} \left( \mathcal{N}^c(\tilde{\beta}_j; \mathcal{V}(\xi_{i,\varepsilon}, \varepsilon), I), \mathcal{N}^c(\tilde{\beta}_j; \mathcal{V}(\xi_{k,\varepsilon}, \varepsilon), I) \right) \leq c_2(I)B^{2j} + o(B^{2j}), \quad (1.4)$$

where  $c_1(I), c_2(I)$  are uniformly bounded for every  $I \subset \mathbb{R}$ .

As in [8], let us introduce also the two-point correlation function  $K_{2,j}$ , which is given by

$$\begin{aligned} K_{2,j}(x, y; t_1, t_2) &= \mathbb{E} \left[ \left| \nabla^2 \tilde{\beta}_j(x) \right| \cdot \left| \nabla^2 \tilde{\beta}_j(y) \right| \mid \nabla \tilde{\beta}_j(x) = \nabla \tilde{\beta}_j(y) = 0, \tilde{\beta}_j(x) = t_1, \tilde{\beta}_j(y) = t_2 \right] \\ &\quad \times \varphi_{x,y}(t_1, t_2, 0, 0, 0, 0) \end{aligned} \quad (1.5)$$



where  $t_1, t_2 \in \mathbb{R}$  and  $\varphi_{x,y}(t_1, t_2, 0, 0, 0, 0)$  denotes the density of the 6-dimensional vector

$$\left( \tilde{\beta}_j(x), \tilde{\beta}_j(y), \nabla \tilde{\beta}_j(x), \nabla \tilde{\beta}_j(y) \right)$$

in  $\tilde{\beta}_j(x) = t_1, \tilde{\beta}_j(y) = t_2, \nabla \tilde{\beta}_j(x) = \nabla \tilde{\beta}_j(y) = \mathbf{0}$ . Note that, by isotropy, the function  $K_{2,j}$  depends on the points  $x, y$  only through their geodesic distance  $\phi = d(x, y)$ ; with some abuse of notation, we shall write

$$K_{2,j}(\phi; t_1, t_2) = K_{2,j}(x, y; t_1, t_2).$$

We are now in the position to investigate the asymptotic behaviour of the long- and short-range components, respectively.

## A.2 Proof of the long-range asymptotic bound (1.3)

By the Kac-Rice expectation metatheorem (see i.e., [1], Chapter 11), we have

$$\begin{aligned} & \sum_{d(\mathcal{V}(\xi_{i,\varepsilon}), \mathcal{V}(\xi_{k,\varepsilon})) > C/B^j} \text{Cov} \left( \mathcal{N}^c(\tilde{\beta}_j; \mathcal{V}(\xi_{i,\varepsilon}), I), \mathcal{N}^c(\tilde{\beta}_j; \mathcal{V}(\xi_{k,\varepsilon}), I) \right) \\ &= \int_{\mathcal{W}} \int_{I \times I} K_{2,j}(x, y; t_1, t_2) dt_1 dt_2 dx dy - \mathbb{E}[\mathcal{N}^c(\tilde{\beta}_j; \mathcal{V}(\xi_{i,\varepsilon}), I)] \mathbb{E}[\mathcal{N}^c(\tilde{\beta}_j; \mathcal{V}(\xi_{k,\varepsilon}), I)] \end{aligned}$$

where

$$\mathcal{W} = \bigcup_{d(\mathcal{V}(\xi_{i,\varepsilon}), \mathcal{V}(\xi_{k,\varepsilon})) > C/B^j} \mathcal{V}(\xi_{i,\varepsilon}) \times \mathcal{V}(\xi_{k,\varepsilon}),$$

is the union of Voronoi cells which are further away than  $C/B^j$ . Our next result is a convenient expression for the expectation; here and in the sequel, we use the simplified notation

$$\mathcal{B}_{2n} = \mathcal{B}_{2n,j} = \mathcal{B}_{2n,p,j},$$

where  $\mathcal{B}_{2n,p,j}$  was introduced in (3.13).

### Lemma A.2

$$\mathbb{E}[\mathcal{N}_I^c(\tilde{\beta}_j(x))] = \frac{1}{2} \frac{\mathcal{B}_{4,j}}{\mathcal{B}_{2,j}} \int_I p(t) dt,$$

where the function  $p$  is defined in (1.6).

**Proof** Let  $\mathcal{N}_I^c(\tilde{\beta}_j)$  be the number of critical points with value in  $I$

$$\mathcal{N}_I^c(\tilde{\beta}_j) = \#\{x \in S^2 : \tilde{\beta}_j(x) \in I, \nabla \tilde{\beta}_j(x) = 0\}.$$

From isotropy and Kac-Rice metatheorem we immediately get that

$$\mathbb{E}[\mathcal{N}_I^c(\tilde{\beta}_j(x))] = 4\pi \int_{\mathbb{R}^4} |\zeta_1 \zeta_3 - \zeta_2^2| \mathbb{1}_{\{t \in I\}} D_j(t, 0, 0, \zeta_1, \zeta_2, \zeta_3) dt d\zeta_1 d\zeta_2 d\zeta_3$$

where  $D_j(t, 0, 0, \zeta_1, \zeta_2, \zeta_3)$  denotes the joint density of  $(\tilde{\beta}_j(x), \nabla \tilde{\beta}_j(x), \nabla^2 \tilde{\beta}_j(x))$  in  $\tilde{\beta}_j(x) = t$ ,  $\nabla \tilde{\beta}_j(x) = \mathbf{0}$ ,  $\nabla^2 \tilde{\beta}_j(x) = (\zeta_1, \zeta_2, \zeta_3) = \zeta$ . Since, at each fixed  $x$ , first and second derivatives are uncorrelated we have

$$D_j(t, 0, 0, \zeta_1, \zeta_2, \zeta_3) = D_{j,1}(0, 0)D_{j,2}(t)D_{j,3}(\zeta_1, \zeta_2, \zeta_3 | \tilde{\beta}_j(x) = t),$$

where  $D_{j,1}$ ,  $D_{j,2}$  and  $D_{j,3}$  are the marginal densities of  $\nabla \tilde{\beta}_j(x)$ ,  $\tilde{\beta}_j(x)$  and  $(\nabla^2 \tilde{\beta}_j(x) | \tilde{\beta}_j(x) = t)$  respectively. In view of the results in Section B, we immediately have that

$$D_{j,1}(0, 0) = \frac{1}{2\pi} \frac{1}{\sqrt{\frac{1}{4}\mathcal{B}_{2,j}^2}} = \frac{1}{2\pi} \frac{1}{\frac{\mathcal{B}_{2,j}}{2}}, \quad D_{j,2}(t) = \frac{1}{\sqrt{2\pi}} e^{-\frac{t^2}{2}},$$

and

$$D_{j,3}(\zeta_1, \zeta_2, \zeta_3 | \tilde{\beta}_j(x) = t) = \frac{1}{(2\pi)^{3/2} \sqrt{\det(\omega_j)}} \exp\left\{-\frac{1}{2}(\zeta - \mu_j(t))\omega_j^{-1}(\zeta - \mu_j(t))^t\right\}$$

where

$$\mu_j(t) = \begin{pmatrix} -\frac{t}{2}\mathcal{B}_{2,j} \\ 0 \\ -\frac{t}{2}\mathcal{B}_{2,j} \end{pmatrix}, \quad \omega_j = \begin{pmatrix} \frac{3}{8}\mathcal{B}_{4,j} - \frac{1}{4}\mathcal{B}_{2,j} - \frac{1}{4}\mathcal{B}_{2,j}^2 & 0 & \frac{1}{8}\mathcal{B}_{4,j} + \frac{1}{4}\mathcal{B}_{2,j} - \frac{1}{4}\mathcal{B}_{2,j}^2 \\ 0 & \frac{1}{8}\mathcal{B}_{4,j} - \frac{1}{4}\mathcal{B}_{2,j} & 0 \\ \frac{1}{8}\mathcal{B}_{4,j} + \frac{1}{4}\mathcal{B}_{2,j} - \frac{1}{4}\mathcal{B}_{2,j}^2 & 0 & \frac{3}{8}\mathcal{B}_{4,j} - \frac{1}{4}\mathcal{B}_{2,j} - \frac{1}{4}\mathcal{B}_{2,j}^2 \end{pmatrix}.$$

With the scaling  $\frac{\sqrt{8}}{\sqrt{\mathcal{B}_{4,j}}}(\nabla^2 \tilde{\beta}_j | \tilde{\beta}_j) \sim N(\tilde{\mu}_j(t), \tilde{\omega}_j)$ , where  $\tilde{\mu}_j(t) = \frac{\sqrt{8}}{\sqrt{\mathcal{B}_{4,j}}}\mu_j(t)$  and  $\tilde{\omega}_j = \frac{8}{\mathcal{B}_{4,j}}\omega_j$ , we obtain

$$\begin{aligned} & D_j(t, 0, 0, \zeta_1, \zeta_2, \zeta_3) dt d\zeta_1 d\zeta_2 d\zeta_3 \\ &= \frac{1}{2\pi} \frac{1}{\frac{\mathcal{B}_2}{2}} \frac{1}{\sqrt{2\pi}} e^{-\frac{t^2}{2}} \frac{1}{(2\pi)^{3/2} \sqrt{\det(\tilde{\omega}_j)}} \exp\left\{-\frac{1}{2}(\tilde{\zeta} - \tilde{\mu}_j(t))\tilde{\omega}_j^{-1}(\tilde{\zeta} - \tilde{\mu}_j(t))^t\right\} dt d\tilde{\zeta}_1 d\tilde{\zeta}_2 d\tilde{\zeta}_3 \end{aligned}$$

and then

$$\int_{\mathbb{R}^4} |\zeta_1 \zeta_3 - \zeta_2^2| \mathbb{1}_{\{t \in I\}} D_j(t, 0, 0, \zeta_1, \zeta_2, \zeta_3) dt d\zeta_1 d\zeta_2 d\zeta_3 = \frac{\mathcal{B}_{4,j}}{8} \frac{1}{\mathcal{B}_{2,j}^2} \frac{1}{2\pi} \int_I p(t) dt,$$

with

$$p(t) = \frac{1}{\sqrt{2\pi}} \frac{1}{(2\pi)^{3/2}} \frac{1}{\sqrt{\det(\tilde{\omega}_j)}} \int_{\mathbb{R}^3} |\tilde{\zeta}_1 \tilde{\zeta}_3 - \tilde{\zeta}_2^2| e^{-\frac{t^2}{2}} \exp\left\{-\frac{1}{2}(\tilde{\zeta} - \tilde{\mu}_j(t))\tilde{\omega}_j^{-1}(\tilde{\zeta} - \tilde{\mu}_j(t))^t\right\} d\tilde{\zeta}_1 d\tilde{\zeta}_2 d\tilde{\zeta}_3. \quad (1.6)$$

□

In order to bound the variance we need to prove the following:

$$\begin{aligned} & 16\pi^2 \iint_{I \times I} \int_{C/B^j}^{\frac{\pi}{2}} K_{2,j}(\phi; t_1, t_2) \sin \phi d\phi dt_1 dt_2 - \frac{1}{4} \frac{\mathcal{B}_{4,j}^2}{\mathcal{B}_{2,j}^2} \iint_{I \times I} p(t_1) p(t_2) dt_1 dt_2 \\ & \leq c_1(I) j^2 B^{2j} + o(j^2 B^{2j}) \end{aligned} \quad (1.7)$$

as  $j \rightarrow \infty$ . The idea of the proof is to give a Taylor expansion of the difference between the two integrands in (1.7), see [8] for a related argument. More precisely, we start by giving the explicit expression of  $K_{2,j}$  in terms of a Gaussian integral; indeed we write, for  $\phi \geq C/B^j$ ,

$$K_{2,j}(\phi; t_1, t_2) = \iint_{\mathbb{R}^3 \times \mathbb{R}^3} |\zeta_{x,1}\zeta_{x,3} - \zeta_{x,2}^2| |\zeta_{y,1}\zeta_{y,3} - \zeta_{y,2}^2| \\ \times D_{j,x,y}(t_1, t_2, 0, 0, 0, 0, \zeta_{x,1}, \zeta_{x,2}, \zeta_{x,3}, \zeta_{y,1}, \zeta_{y,2}, \zeta_{y,3}) d\zeta_{x,1} d\zeta_{x,2} d\zeta_{x,3} d\zeta_{y,1} d\zeta_{y,2} d\zeta_{y,3}$$

where  $D_{j,x,y}$  denotes the joint density of  $(\tilde{\beta}_j(x), \tilde{\beta}_j(y), \nabla \tilde{\beta}_j(x), \nabla \tilde{\beta}_j(y), \nabla^2 \tilde{\beta}_j(x), \nabla^2 \tilde{\beta}_j(y))$ . We have also

$$D_{j,x,y}(t_1, t_2, \mathbf{0}, \mathbf{0}, \zeta_x, \zeta_y) = D_{j,x,y,1}(\mathbf{0}, \mathbf{0}) D_{j,x,y,2}(t_1, t_2 | \nabla \tilde{\beta}_j(x) = \nabla \tilde{\beta}_j(y) = \mathbf{0}) \\ \times D_{j,x,y,3}(\zeta_x, \zeta_y | \tilde{\beta}_j(x) = t_1, \tilde{\beta}_j(y) = t_2, \nabla \tilde{\beta}_j(x) = \nabla \tilde{\beta}_j(y) = \mathbf{0})$$

where  $D_{j,x,y,1}$  is the density of  $(\nabla \tilde{\beta}_j(x), \nabla \tilde{\beta}_j(y))$  and  $D_{j,x,y,2}$ ,  $D_{j,x,y,3}$  are the conditional densities of  $(\tilde{\beta}_j(x), \tilde{\beta}_j(y) | \nabla \tilde{\beta}_j(x) = \nabla \tilde{\beta}_j(y) = \mathbf{0})$  and  $(\nabla^2 \tilde{\beta}_j(x), \nabla^2 \tilde{\beta}_j(y) | \tilde{\beta}_j(x) = t_1, \tilde{\beta}_j(y) = t_2, \nabla \tilde{\beta}_j(x) = \nabla \tilde{\beta}_j(y) = \mathbf{0})$  respectively.

In order to investigate the asymptotic behaviour of these densities, we need first to write the block components of the full covariance matrix of the field and its (first and second order) derivatives. In particular, we introduce the following notation for the matrix  $\Sigma_j(\phi(x, y)) = \Sigma_j(\phi)$ :

$$\Sigma_j(\phi) = \begin{pmatrix} R_j(\phi) & E_j(\phi) & D_j(\phi) \\ E_j^T(\phi) & A_j(\phi) & B_j(\phi) \\ D_j^T(\phi) & B_j^T(\phi) & C_j(\phi) \end{pmatrix}.$$

Here,  $R_j(\phi(x, y))$  is the  $2 \times 2$  covariance matrix of  $(\tilde{\beta}_j(x), \tilde{\beta}_j(y))$ ;  $E_j(\phi)$  is the  $2 \times 4$  covariance matrix between  $(\tilde{\beta}_j(x), \tilde{\beta}_j(y))$  and  $(\nabla \tilde{\beta}_j(x), \nabla \tilde{\beta}_j(y))$ ;  $D_j(\phi)$  is the  $2 \times 6$  covariance matrix between  $(\tilde{\beta}_j(x), \tilde{\beta}_j(y))$  and  $(\nabla^2 \tilde{\beta}_j(x), \nabla^2 \tilde{\beta}_j(y))$ ;  $A_j(\phi)$  is the  $4 \times 4$  covariance matrix of  $(\nabla \tilde{\beta}_j(x), \nabla \tilde{\beta}_j(y))$ ;  $B_j(\phi)$  is the  $4 \times 6$  covariance matrix between  $(\nabla \tilde{\beta}_j(x), \nabla \tilde{\beta}_j(y))$  and  $(\nabla^2 \tilde{\beta}_j(x), \nabla^2 \tilde{\beta}_j(y))$ ; and finally for  $C_j(\phi)$  is the  $6 \times 6$  covariance matrix of the vector  $(\nabla^2 \tilde{\beta}_j(x), \nabla^2 \tilde{\beta}_j(y))$  (see Appendix B).

With this notation in mind, can easily give the value of the bivariate density for levels, evaluated at the origin; we have

$$D_{j,x,y,1}(\mathbf{0}, \mathbf{0}) = \frac{1}{\pi^2 \mathcal{B}_2^2} \frac{1}{\sqrt{(1 - 4\frac{\alpha_1^2}{\mathcal{B}_2^2})(1 - 4\frac{\alpha_2^2}{\mathcal{B}_2^2})}},$$

where  $\alpha_1 = \alpha_{1,j}(\phi)$  and  $\alpha_2 = \alpha_{2,j}(\phi)$  are elements of the covariance matrix  $A_j(\phi)$ , whose analytic expression is given below in (2.1) and (2.2). On the other hand, we have also the conditional densities

$$D_{j,x,y,2}(t_1, t_2 | \nabla \tilde{\beta}_j(x) = \nabla \tilde{\beta}_j(y) = \mathbf{0}) = \frac{1}{2\pi} \frac{1}{\sqrt{\det(\Sigma_{2,j}(\phi))}} \exp\{-\frac{1}{2}(t_1, t_2) \Sigma_{2,j}^{-1}(\phi) (t_1, t_2)^T\},$$

where

$$\Sigma_{2,j}(\phi) = R_j(\phi) - E_j(\phi)A_j^{-1}(\phi)E_j^T(\phi).$$

Moreover

$$\begin{aligned} & D_{j,x,y,3}(\zeta_x, \zeta_y | \tilde{\beta}_j(x) = t_1, \tilde{\beta}_j(y) = t_2, \nabla \tilde{\beta}_j(x) = \nabla \tilde{\beta}_j(y) = \mathbf{0}) \\ &= \frac{1}{(2\pi)^3} \frac{1}{\sqrt{\det(\Omega_j(\phi))}} \exp \left\{ -\frac{1}{2} ((\zeta_x, \zeta_y) - \mu_j(\phi, t_1, t_2)) \Omega_j(\phi)^{-1} ((\zeta_x, \zeta_y) - \mu_j(\phi, t_1, t_2))^T \right\} \end{aligned}$$

where the mean vector and covariance matrix are given by

$$\mu_j(\phi, t_1, t_2) = \begin{pmatrix} D_j(\phi)^T & B_j(\phi)^T \end{pmatrix} \begin{pmatrix} R_j(\phi) & E_j(\phi) \\ E_j(\phi)^T & A_j(\phi) \end{pmatrix}^{-1} \begin{pmatrix} t_1 \\ t_2 \\ \mathbf{0} \\ \mathbf{0} \end{pmatrix}$$

and

$$\Omega_j(\phi) = C_j(\phi) - \begin{pmatrix} D_j(\phi)^T & B_j(\phi)^T \end{pmatrix} \begin{pmatrix} R_j(\phi) & E_j(\phi) \\ E_j(\phi)^T & A_j(\phi) \end{pmatrix}^{-1} \begin{pmatrix} D_j(\phi) \\ B_j(\phi) \end{pmatrix},$$

respectively. After the change of variables

$$\frac{\sqrt{8}}{\sqrt{\mathcal{B}_{4,j}}}(\zeta_x, \zeta_y) = (\tilde{\zeta}_x, \tilde{\zeta}_y),$$

we have

$$\begin{aligned} & D_{j,x,y,3}(\zeta_x, \zeta_y | \tilde{\beta}_j(x) = t_1, \tilde{\beta}_j(y) = t_2, \nabla \tilde{\beta}_j(x) = \nabla \tilde{\beta}_j(y) = \mathbf{0}) d\zeta_x d\zeta_y \\ &= \frac{1}{(2\pi)^3} \frac{1}{\sqrt{\det(\Delta_j(\phi))}} \exp \left\{ -\frac{1}{2} ((\tilde{\zeta}_x, \tilde{\zeta}_y) - \tilde{\mu}_j(\phi, t_1, t_2)) \Delta_j(\phi)^{-1} ((\tilde{\zeta}_x, \tilde{\zeta}_y) - \tilde{\mu}_j(\phi, t_1, t_2))^T \right\} d\tilde{\zeta}_x d\tilde{\zeta}_y \end{aligned}$$

where

$$\Delta_j(\phi) = \frac{8}{\mathcal{B}_{4,j}} \Omega_j(\phi).$$

The idea to conclude the proof is to write all the covariance matrix involved as (small) perturbations of their limiting values. For definiteness and simplicity, we consider the case where  $2 < \gamma < 6$  and  $p = 1$ ; all the other parameter ranges can be dealt in an entirely analogous way, provided that  $\gamma < 4p + 2$ , as usually required for Mexican needlets. In particular, with a hard computation (which can be assisted by a computer), it is possible to show that the covariance matrix is given by

$$\Delta_j(\phi) = \begin{pmatrix} \Delta_{1,j}(\phi) & \Delta_{2,j}(\phi) \\ \Delta_{2,j}(\phi) & \Delta_{1,j}(\phi) \end{pmatrix},$$

with

$$\Delta_{1,j}(\phi) = \begin{pmatrix} 3 - v(\gamma) & 0 & 1 - v(\gamma) \\ 0 & 1 & 0 \\ 1 - v(\gamma) & 0 & 3 - v(\gamma) \end{pmatrix} + \begin{pmatrix} \tilde{a}_{1,j}(\phi) - 2\frac{\mathcal{B}_{2,j}^2}{\mathcal{B}_{4,j}} + v(\gamma) & 0 & \tilde{a}_{4,j}(\phi) - 2\frac{\mathcal{B}_{2,j}^2}{\mathcal{B}_{4,j}} + v(\gamma) \\ 0 & \tilde{a}_{2,j}(\phi) & 0 \\ \tilde{a}_{4,j}(\phi) - 2\frac{\mathcal{B}_{2,j}^2}{\mathcal{B}_{4,j}} + v(\gamma) & 0 & \tilde{a}_{3,j}(\phi) - 2\frac{\mathcal{B}_{2,j}^2}{\mathcal{B}_{4,j}} + v(\gamma) \end{pmatrix},$$

$$\Delta_{2,j}(\phi) = \begin{pmatrix} \tilde{a}_{5,j}(\phi) & 0 & \tilde{a}_{8,j}(\phi) \\ 0 & \tilde{a}_{6,j}(\phi) & 0 \\ \tilde{a}_{8,j}(\phi) & 0 & \tilde{a}_{7,j}(\phi) \end{pmatrix},$$

where we note that in view of (3.14), for  $\gamma \in (2, 6)$ , we have

$$2\frac{\mathcal{B}_{2,j}^2}{\mathcal{B}_{4,j}} = v(\gamma) + O(B^{-2j}), \quad v(\gamma) = 2\frac{6-\gamma}{8-\gamma} \in (0, 4/3).$$

Likewise

$$\Sigma_{2,j}(\phi) = \begin{pmatrix} 1 & 0 \\ 0 & 1 \end{pmatrix} + \begin{pmatrix} a_{1,j}(\phi) & a_{2,j}(\phi) \\ a_{2,j}(\phi) & a_{1,j}(\phi) \end{pmatrix}.$$

In the previous formulae, we have introduced the vectors  $\mathbf{a}$  and  $\tilde{\mathbf{a}}$  that collect the perturbing elements of the covariance matrices  $\Sigma_{2,j}(\phi)$  and  $\Delta_j(\phi)$  respectively, i.e.,

$$\mathbf{a} = \mathbf{a}_j(\phi) = (a_{1,j}(\phi), a_{2,j}(\phi)), \quad \tilde{\mathbf{a}} = \tilde{\mathbf{a}}_j(\phi) = (\tilde{a}_{1,j}(\phi), \dots, \tilde{a}_{8,j}(\phi)).$$

In view of Lemma B.2, these elements are such that there exists a constant  $K_M > 0$

$$a_{k,j}(\phi), \tilde{a}_{i,j}(\phi) \leq \frac{K_M}{(1 + j^{-1}B^j\phi)^M}, \quad k = 1, 2, i = 1, \dots, 8.$$

In what follows, with a slight abuse of notation, we write the conditional covariance matrices  $\Sigma_{j,2}(\phi)$  and  $\Delta_j(\phi)$  as a function of  $\mathbf{a}$  and  $\tilde{\mathbf{a}}$ , and the 2-point correlation function  $K_{2,j}$  as a function of the perturbing elements  $a_{k,j}(\phi)$ ,  $k = 1, 2$  and  $\tilde{a}_{i,j}(\phi)$ ,  $i = 1, \dots, 8$ . It is a classical result of perturbation theory (see i.e., [20]) that Gaussian expectations are analytic functions of the perturbing elements  $a_{k,j}(\phi)$  and  $\tilde{a}_{i,j}(\phi)$ , so we can expand them into a Taylor polynomial around  $\mathbf{0}$ . In particular, let

$$q(\mathbf{a}; t_1, t_2) = \frac{1}{\sqrt{\det(\Sigma_{2,j}(\mathbf{a}))}} \exp\left\{-\frac{1}{2}(t_1, t_2)\Sigma_{2,j}^{-1}(\mathbf{a})(t_1, t_2)^T\right\} \quad (1.8)$$

and

$$\tilde{q}(\tilde{\mathbf{a}}; t_1, t_2) = \frac{1}{\sqrt{\det(\Delta_j(\tilde{\mathbf{a}}))}} \exp\left\{-\frac{1}{2}((\tilde{\zeta}_x, \tilde{\zeta}_y) - \tilde{\mu}_j(\phi, t_1, t_2))\Delta_j(\tilde{\mathbf{a}})^{-1}((\tilde{\zeta}_x, \tilde{\zeta}_y) - \tilde{\mu}_j(\phi, t_1, t_2))^T\right\}.$$

As  $\|\mathbf{a}\| \rightarrow 0$  we have the expansions

$$q(\mathbf{a}; t_1, t_2) = q(\mathbf{0}; t_1, t_2) + \sum_{i=1}^2 a_i \frac{\partial}{\partial a_i} q(\mathbf{0}; t_1, t_2) + a_1 a_2 \frac{\partial^2}{\partial a_1 \partial a_2} q(\mathbf{0}; t_1, t_2) \\ + \frac{1}{2} \sum_{i=1}^2 a_i^2 \frac{\partial^2}{\partial a_i^2} q(\mathbf{0}; t_1, t_2) + O(r(t_1, t_2)\|\mathbf{a}\|^3), \quad (1.9)$$

and

$$\begin{aligned}\tilde{q}(\tilde{\mathbf{a}}; t_1, t_2) &= \tilde{q}(\mathbf{0}; t_1, t_2) + \sum_{i=1}^8 \tilde{a}_i \frac{\partial}{\partial \tilde{a}_i} \tilde{q}(\mathbf{0}; t_1, t_2) + \sum_{i \neq j} \tilde{a}_i \tilde{a}_j \frac{\partial^2}{\partial \tilde{a}_i \partial \tilde{a}_j} \tilde{q}(\mathbf{0}; t_1, t_2) \\ &\quad + \frac{1}{2} \sum_{i=1}^8 \tilde{a}_i^2 \frac{\partial^2}{\partial \tilde{a}_i^2} \tilde{q}(\mathbf{0}; t_1, t_2) + O(r(t_1, t_2) \|\tilde{\mathbf{a}}\|^3).\end{aligned}$$

In view of Lemma B.2 and the analytic expressions of the perturbing elements  $a_i$  and  $\tilde{a}_i$  we immediately have the following bounds

$$\int_{C/B^j}^{\pi/2} a_{i,j}(\phi) \sin \phi \, d\phi, \quad \int_{C/B^j}^{\pi/2} \tilde{a}_{k,j}(\phi) \sin \phi \, d\phi = O(j^2 B^{-2j}). \quad (1.10)$$

Now formula (1.7) follows by observing that

$$\begin{aligned}& \frac{16\pi^2}{2^4 8^2 \pi^6} \frac{\mathcal{B}_{4,j}^2}{\mathcal{B}_{2,j}^2} \int_{C/B^j}^{\pi/2} \iint_{\mathbb{R}^3 \times \mathbb{R}^3} |\tilde{\zeta}_{x,1} \tilde{\zeta}_{x,3} - \tilde{\zeta}_{x,2}^2| |\tilde{\zeta}_{y,1} \tilde{\zeta}_{y,3} - \tilde{\zeta}_{y,2}^2| \frac{1}{\sqrt{(1 - 4\frac{\alpha_1^2}{\mathcal{B}_{2,j}^2})(1 - 4\frac{\alpha_2^2}{\mathcal{B}_{2,j}^2})}} q(\mathbf{0}; t_1, t_2) \\ & \quad \times \tilde{q}(\mathbf{0}; t_1, t_2) \sin \phi \, d\phi \, d\tilde{\zeta}_{x,1} d\tilde{\zeta}_{x,2} d\tilde{\zeta}_{x,3} d\tilde{\zeta}_{y,1} d\tilde{\zeta}_{y,2} d\tilde{\zeta}_{y,3} - \frac{1}{4} \frac{\mathcal{B}_{4,j}^2}{\mathcal{B}_{2,j}^2} p(t_1) p(t_2) \\ & \leq c_1(t_1, t_2) \frac{\mathcal{B}_{4,j}^2}{\mathcal{B}_{2,j}^2} j^2 B^{-2j},\end{aligned}$$

because the leading terms cancel with the centring factor, and all the other components are bounded in view of (1.8), (1.9) and (1.10). This concludes the analysis of the long-range components.

### A.3 Proof of the short-range asymptotic bound (1.4)

We bound now the contribution of the terms that are at a smaller distance than  $C/B^j$ . As in [8], we can use again the Kac-Rice metatheorem to show that there exists a constant  $c > 0$  such that for every nice domain  $\mathcal{D} \subseteq \mathbb{S}^2$  contained in some spherical cap of radius  $c/B^j$ , one has

$$\mathbb{E}[\mathcal{N}^c(\tilde{\beta}_j; \mathcal{D}, I)(\mathcal{N}^c(\tilde{\beta}_j; \mathcal{D}, I) - 1)] = \iint_{\mathcal{D} \times \mathcal{D}} \iint_{I \times I} K_{2,j}(x, y; t_1, t_2) dt_1 dt_2 dx dy. \quad (1.11)$$

Let

$$\varepsilon = c/B^j; \quad (1.12)$$

then we have

$$\begin{aligned}\text{Var} \left( \mathcal{N}^c(\tilde{\beta}_j; \mathcal{V}(\xi_{\varepsilon,i}), I) \right) &= \iint_{\mathcal{V}(\xi_{\varepsilon,i}) \times \mathcal{V}(\xi_{\varepsilon,i})} \iint_{I \times I} K_{2,j}(x, y; t_1, t_2) dt_1 dt_2 dx dy \\ &\quad + \mathbb{E} \left[ \mathcal{N}^c(\tilde{\beta}_j; \mathcal{V}(\xi_{\varepsilon,i}), I) \right] - \left( \mathbb{E} \left[ \mathcal{N}^c(\tilde{\beta}_j; \mathcal{V}(\xi_{\varepsilon,i}), I) \right] \right)^2.\end{aligned} \quad (1.13)$$

It is easy to see that

$$\mathbb{E} \left[ \mathcal{N}^c(\tilde{\beta}_j; V(\xi_{\varepsilon,i}), I) \right] \leq \mathbb{E} \left[ \mathcal{N}^c(\tilde{\beta}_j; B(\xi_{\varepsilon,i}; \varepsilon), I) \right] \leq \pi \varepsilon^2 B^{2j} = O(1), \quad (1.14)$$

by (1.12). Moreover we have the following result

**Lemma A.3** *There exists a constant  $c > 0$  such that, for  $d(x, y) < c/B^j$ , one has*

$$\iint_{I \times I} K_{2,j}(x, y; t_1, t_2) dt_1 dt_2 \leq O(B^{4j})$$

with the constant involved in the  $O$ -notation universal.

**Proof** Since  $K_{2,j}(x, y; t_1, t_2)$  is nonnegative for all the values of its arguments, it is enough to study the rate of the following uniform bound in  $I$ :

$$K_{2,j}(\phi, \mathbb{R}, \mathbb{R}) = \iint_{\mathbb{R} \times \mathbb{R}} K_{2,j}(\phi; t_1, t_2) dt_1 dt_2;$$

for  $\phi < c/B^j$ . With the change of variable  $\phi = \psi/B^j$ , we need to study

$$\begin{aligned} K_{2,j}(\psi; \mathbb{R}, \mathbb{R}) &= \frac{1}{(2\pi)^2} \frac{1}{\sqrt{\det(A_j(\psi))}} \frac{B_{4,j}^2}{8^2} \iint_{\mathbb{R}^3 \times \mathbb{R}^3} |\tilde{\zeta}_{x,1} \tilde{\zeta}_{x,3} - \tilde{\zeta}_{x,2}^2| |\tilde{\zeta}_{y,1} \tilde{\zeta}_{y,3} - \tilde{\zeta}_{y,2}^2| \\ &\quad \times \frac{1}{(2\pi)^3} \frac{1}{\sqrt{\det(H_j(\psi))}} \exp \left\{ -\frac{1}{2} \tilde{\zeta} H_j(\psi)^{-1} \tilde{\zeta}^t \right\} d\tilde{\zeta}_{x,1} d\tilde{\zeta}_{x,2} d\tilde{\zeta}_{x,3} d\tilde{\zeta}_{y,1} d\tilde{\zeta}_{y,2} d\tilde{\zeta}_{y,3}. \end{aligned}$$

First note that

$$\begin{aligned} \frac{1}{\sqrt{\det(A_j(\psi))}} &= \frac{1}{(2\pi)^2} \frac{1}{\frac{1}{4} \frac{1}{2^{4j}} B_{2,j}^2 \sqrt{(1 - 2^2 2^{4j} \alpha_1^2(\psi)/B_{2,j}^2)(1 - 2^2 2^{4j} \alpha_2^2(\psi)/B_{2,j}^2)}} \\ &\leq \frac{1}{(2\pi)^2} \frac{1}{\frac{1}{4} \frac{1}{2^{4j}} B_{2,j}^2 \sqrt{(1 - 2 2^{2j} \alpha_1(\psi)/B_{2,j})(1 - 2 2^{2j} \alpha_2(\psi)/B_{2,j})}} \end{aligned}$$

and by Taylor expanding  $\alpha_1$  and  $\alpha_2$  (which again can be assisted by a computer), we obtain

$$(1 - 2 2^{2j} \alpha_1(\psi)/B_2)(1 - 2 2^{2j} \alpha_2(\psi)/B_2) = O(\psi^4).$$

It is easy to check that

$$K_{2,j}(\psi; \mathbb{R}, \mathbb{R}) \leq \mathbb{E}[|X_1 X_3| |Y_1 Y_3| + |X_1 X_3| Y_2^2 + |Y_1 Y_3| X_2^2 + Y_2^2 X_2^2]$$

where  $(X_1, X_2, X_3, Y_1, Y_2, Y_3)$  is a centred Gaussian with covariance matrix  $H_j(\psi)$

$$H_j(\psi) = C_j(\psi) - B_j(\psi)^t A_j(\psi)^{-1} B_j(\psi) = \begin{pmatrix} H_{1,j}(\psi) & H_{2,j}(\psi) \\ H_{2,j}(\psi) & H_{1,j}(\psi) \end{pmatrix}$$

Because we shall use a Cauchy-Schwartz bound, it is enough to focus on the blocks on the main diagonal, which we write as

$$H_{1,j}(\psi) = \begin{pmatrix} h_{1,j}(\psi) & 0 & h_{4,j}(\psi) \\ 0 & h_{2,j}(\psi) & 0 \\ h_{4,j}(\psi) & 0 & h_{3,j}(\psi) \end{pmatrix}$$

where the analytic expressions of the  $h_{i,j}(\psi)$  are derived by a computer assisted computation. Now, by Cauchy-Schwartz, we have

$$\begin{aligned} & \mathbb{E}[|X_1 X_3| |Y_1 Y_3| + |X_1 X_3| Y_2^2 + |Y_1 Y_3| X_2^2 + Y_2^2 X_2^2] \\ & \leq 3h_{1,j}(\psi)h_{3,j}(\psi) + 6(h_{1,j}(\psi))^{1/2}(h_{3,j}(\psi))^{1/2}h_{2,j}(\psi) + 3h_{2,j}(\psi)^2. \end{aligned}$$

and by Taylor expanding the  $h_{i,j}(\psi)$  around  $\psi = 0$  (again by a computer assisted computation) we have

$$\begin{aligned} & \mathbb{E}[|X_1 X_3| |Y_1 Y_3| + |X_1 X_3| Y_2^2 + |Y_1 Y_3| X_2^2 + Y_2^2 X_2^2] \\ & \leq \frac{3 \cdot 2^{-18j-7} (2\mathcal{B}_{2,j} - \mathcal{B}_{4,j}) \mathcal{B}_{4,j} \left( 2^{8j+1} \mathcal{B}_{2,j} (6\mathcal{B}_{2,j} - 4\mathcal{B}_{4,j} + 5\mathcal{B}_{6,j}) - 9 \cdot 2^{8j} \mathcal{B}_{4,j}^2 \right) \psi^2}{\mathcal{B}_{2,j} (2\mathcal{B}_{2,j} - 3\mathcal{B}_{4,j})} + O(\psi^3) \end{aligned}$$

so that the numerator is uniformly bounded by terms of order  $\psi^2$  and

$$K_{2,j}(\psi; \mathbb{R}, \mathbb{R}) = \frac{O(\psi^2) \mathcal{B}_{4,j}^2}{O(\psi^2) \mathcal{B}_{2,j}^2} = O(B^{4j}).$$

□

By Lemma A.3, we have

$$\int_{\mathcal{V}(\xi_{\varepsilon,i}) \times \mathcal{V}(\xi_{\varepsilon,i})} \int_{I \times I} K_{2,j}(x, y; t_1, t_2) dt_1 dt_2 dx dy \leq B^{4j} \cdot (\pi\varepsilon^2)^2 = O(1), \quad (1.15)$$

again by (1.12). Substituting the estimates (1.14) and (1.15) into (1.13) yields

$$\text{Var} \left( \mathcal{N}^c(\tilde{\beta}_j; \mathcal{V}(\xi_{\varepsilon,i}), I) \right) = O(1). \quad (1.16)$$

and, by (1.16),

$$\left| \text{Cov} \left( \mathcal{N}^c(\tilde{\beta}_j; \mathcal{V}(\xi_{i,\varepsilon}), I), \mathcal{N}^c(\tilde{\beta}_j; \mathcal{V}(\xi_{j,\varepsilon}), I) \right) \right| \leq O(1). \quad (1.17)$$

As there are  $O(B^{2j})$  pairs of Voronoi cells at distance smaller or equal than  $C/B^j$ , (1.17) implies that the contribution of this range to (1.1) is

$$\sum_{d(\mathcal{V}(\xi_{i,\varepsilon}), \mathcal{V}(\xi_{k,\varepsilon})) \leq C/B^j} \left| \text{Cov} \left( \mathcal{N}^c(\tilde{\beta}_j; \mathcal{V}(\xi_{i,\varepsilon}), I), \mathcal{N}^c(\tilde{\beta}_j; \mathcal{V}(\xi_{k,\varepsilon}), I) \right) \right| = O(B^{2j}).$$



## B Proof of auxiliary results: covariance matrices

In this section we evaluate the covariance matrix  $\Sigma_j(x, y)$  of the 12-dimensional Gaussian vector

$$(\tilde{\beta}_j(x), \tilde{\beta}_j(y), \nabla \tilde{\beta}_j(x), \nabla \tilde{\beta}_j(y), \nabla^2 \tilde{\beta}_j(x), \nabla^2 \tilde{\beta}_j(y)),$$

which combines level, gradient and elements of the Hessian evaluated at  $x$  and  $y$ . The computations do not require sophisticated arguments, other than iterative derivations of Legendre polynomials. Note that  $\Sigma_j(x, y)$  depends only on the geodesic distance  $\phi = d(x, y)$ , so, abusing notation, we shall write  $\Sigma_j(x, y) = \Sigma_j(\phi)$ . It is convenient to write  $\Sigma_j(x, y)$  in block-diagonal form, i.e.

$$\Sigma_j(\phi) = \begin{pmatrix} R_j(\phi) & E_j(\phi) & D_j(\phi) \\ E_j^T(\phi) & A_j(\phi) & B_j(\phi) \\ D_j^T(\phi) & B_j^T(\phi) & C_j(\phi) \end{pmatrix}.$$

In what follows we use the notation

$$b_{\ell,j} = \frac{1}{\sum_{\ell=B^{j-1}}^{B^{j+1}} b_p^2(\frac{\ell}{B^j}) C_\ell \frac{2\ell+1}{4\pi}} b_p^2(\frac{\ell}{B^j}) C_\ell \frac{2\ell+1}{4\pi}.$$

- $R_j(\phi)$  is the covariance matrix of  $(\tilde{\beta}_j(x), \tilde{\beta}_j(y))$ :

$$R_j(\phi)_{2 \times 2} = \begin{pmatrix} 1 & \rho_j(\phi) \\ \rho_j(\phi) & 1 \end{pmatrix}, \quad \rho_j(\phi) = \sum_{\ell=B^{j-1}}^{B^{j+1}} b_{\ell,j} P_\ell(\cos \phi).$$

- $E_j(\phi)$  is the  $2 \times 4$  matrix

$$E_j(x, y)_{2 \times 4} = \begin{pmatrix} 0 & 0 & 0 & \epsilon_j(\phi) \\ 0 & -\epsilon_j(\phi) & 0 & 0 \end{pmatrix}, \quad \epsilon_j(\phi) = \sin \phi \sum_{\ell=B^{j-1}}^{B^{j+1}} b_{\ell,j} P'_\ell(\cos \phi).$$

- $D_j(\phi)$  is given by

$$D_j(x, y)_{2 \times 6} = \begin{pmatrix} -\frac{1}{2} \mathcal{B}_{2,j} & 0 & -\frac{1}{2} \mathcal{B}_{2,j} & -\delta_\ell(\phi) & 0 & -\delta_\ell(\phi) \\ -\delta_\ell(\phi) & 0 & -\delta_\ell(\phi) & -\frac{1}{2} \mathcal{B}_{2,j} & 0 & -\frac{1}{2} \mathcal{B}_{2,j} \end{pmatrix},$$

with elements

$$\delta_\ell(\phi) = \cos \phi \sum_{\ell} b_{\ell,j} P'_\ell(\cos \phi).$$

- $A$  is the  $4 \times 4$  matrix given by

$$A_j(x, y)_{4 \times 4} = \begin{pmatrix} \frac{1}{2}\mathcal{B}_{2,j} & 0 & \alpha_{1,j}(\phi) & 0 \\ 0 & \frac{1}{2}\mathcal{B}_{2,j} & 0 & \alpha_{2,j}(\phi) \\ \alpha_{1,j}(\phi) & 0 & \frac{1}{2}\mathcal{B}_{2,j} & 0 \\ 0 & \alpha_{2,j}(\phi) & 0 & \frac{1}{2}\mathcal{B}_{2,j} \end{pmatrix},$$

where

$$\alpha_{1,j}(\phi) = \sum_{\ell} b_{\ell,j} P'_{\ell}(\cos \phi), \quad (2.1)$$

$$\alpha_{2,j}(\phi) = -\sin^2 \phi \sum_{\ell} b_{\ell,j} P''_{\ell}(\cos \phi) + \cos \phi \sum_{\ell} b_{\ell,j} P'_{\ell}(\cos \phi). \quad (2.2)$$

- $B$  is given by

$$B_j(x, y)_{4 \times 6} = \begin{pmatrix} \mathbf{0} & b_j(\phi) \\ -b_j(\phi) & \mathbf{0} \end{pmatrix}$$

with

$$b_j(\phi) = \begin{pmatrix} 0 & \beta_{1,j}(\phi) & 0 \\ \beta_{2,j}(\phi) & 0 & \beta_{3,j}(\phi) \end{pmatrix},$$

$$\beta_{1,j}(\phi) = \sin \phi \sum_{\ell} b_{\ell,j} P''_{\ell}(\cos \phi),$$

$$\beta_{2,j}(\phi) = \sin \phi \cos \phi \sum_{\ell} b_{\ell,j} P''_{\ell}(\cos \phi) + \sin \phi \sum_{\ell} b_{\ell,j} P'_{\ell}(\cos \phi),$$

$$\beta_{3,j}(\phi) = -\sin^3 \phi \sum_{\ell} b_{\ell,j} P'''_{\ell}(\cos \phi) + 3 \sin \phi \cos \phi \sum_{\ell} b_{\ell,j} P''_{\ell}(\cos \phi) + \sin \phi \sum_{\ell} b_{\ell,j} P'_{\ell}(\cos \phi).$$

- Finally for  $C$  we have

$$C_j(x, y)_{6 \times 6} = \begin{pmatrix} c_j(0) & c_j(\phi) \\ c_j(\phi) & c_j(0) \end{pmatrix}$$

where

$$c_j(0) = \begin{pmatrix} \frac{3}{8}\mathcal{B}_{4,j} - \frac{1}{4}\mathcal{B}_{2,j} & 0 & \frac{1}{8}\mathcal{B}_{4,j} + \frac{1}{4}\mathcal{B}_{2,j} \\ 0 & \frac{1}{8}\mathcal{B}_{4,j} - \frac{1}{4}\mathcal{B}_{2,j} & 0 \\ \frac{1}{8}\mathcal{B}_{4,j} + \frac{1}{4}\mathcal{B}_{2,j} & 0 & \frac{3}{8}\mathcal{B}_{4,j} - \frac{1}{4}\mathcal{B}_{2,j} \end{pmatrix},$$

and

$$c_j(\phi) = \begin{pmatrix} \gamma_{1,j}(\phi) & 0 & \gamma_{3,j}(\phi) \\ 0 & \gamma_{2,j}(\phi) & 0 \\ \gamma_{3,j}(\phi) & 0 & \gamma_{4,j}(\phi) \end{pmatrix},$$

with

$$\begin{aligned}
\gamma_{1,j}(\phi) &= (2 + \cos^2 \phi) \sum_{\ell} b_{\ell,j} P_{\ell}''(\cos \phi) + \cos \phi \sum_{\ell} b_{\ell,j} P_{\ell}'(\cos \phi) \\
\gamma_{2,j}(\phi) &= -\sin^2 \phi \sum_{\ell} b_{\ell,j} P_{\ell}'''(\cos \phi) + \cos \phi \sum_{\ell} b_{\ell,j} P_{\ell}''(\cos \phi) \\
\gamma_{3,j}(\phi) &= -\sin^2 \phi \cos \phi \sum_{\ell} b_{\ell,j} P_{\ell}'''(\cos \phi) + (-2 \sin^2 \phi + \cos^2 \phi) \sum_{\ell} b_{\ell,j} P_{\ell}''(\cos \phi) \\
&\quad + \cos \phi \sum_{\ell} b_{\ell,j} P_{\ell}'(\cos \phi), \\
\gamma_{4,j}(\phi) &= \sin^4 \phi \sum_{\ell} b_{\ell,j} P_{\ell}''''(\cos \phi) - 6 \sin^2 \phi \cos \phi \sum_{\ell} b_{\ell,j} P_{\ell}'''(\cos \phi) \\
&\quad + (-4 \sin^2 \phi + 3 \cos^2 \phi) \sum_{\ell} b_{\ell,j} P_{\ell}''(\cos \phi) + \cos \phi \sum_{\ell} b_{\ell,j} P_{\ell}'(\cos \phi).
\end{aligned}$$

It is a well-known fact in the theory of stationary and isotropic stochastic processes that the covariance of derivative fields can be evaluated by means of derivatives of the covariance functions; this issue is discussed for instance in [1], p. 268. Hence, for the results to follow, we shall need to control the asymptotic behaviour of higher-order derivatives of this covariance function. These results are collected in the following Proposition.

**Proposition B.1** *For all nonnegative integers  $a, b, c, d \in \mathbb{N}_+$ , there exist  $K > 0$  such that, for all  $x, y \in S^2$*

$$\frac{\partial^a}{\partial \theta_x^a} \frac{\partial^b}{\partial \theta_y^b} \frac{\partial^c}{\partial \phi_x^c} \frac{\partial^d}{\partial \phi_y^d} \mathbb{E}[\tilde{\beta}_j(x) \tilde{\beta}_{j,p}(y)] \leq B^{j(a+b+c+d)} \frac{K}{(1 + j^{-1} B^j d(x, y))^{4p+2-\gamma}}.$$

**Proof** The result is a simple consequence of equation (8) in [16], from which we have that

$$\begin{aligned}
\frac{\partial^a}{\partial \theta_x^a} \frac{\partial^b}{\partial \theta_y^b} \frac{\partial^c}{\partial \phi_x^c} \frac{\partial^d}{\partial \phi_y^d} \mathbb{E}[\beta_j(x) \beta_j(y)] &= \sum_{\ell=1}^{\infty} b^2 \left( \frac{\ell}{B^j}; p \right) C_{\ell} \frac{2\ell+1}{4\pi} \frac{\partial^a}{\partial \theta_x^a} \frac{\partial^b}{\partial \theta_y^b} \frac{\partial^c}{\partial \phi_x^c} \frac{\partial^d}{\partial \phi_y^d} P_{\ell}(\langle x, y \rangle) \\
&\leq B^{j(a+b+c+d)} \frac{K_M}{(1 + j^{-1} B^j d(x, y))^{4p+2-\gamma}} \sum_{\ell=1}^{\infty} b^2 \left( \frac{\ell}{B^j}; p \right) C_{\ell} \frac{2\ell+1}{4\pi},
\end{aligned}$$

$a, b, c, d \in \mathbb{N}$ , so that

$$\frac{\partial^a}{\partial \theta_x^a} \frac{\partial^b}{\partial \theta_y^b} \frac{\partial^c}{\partial \phi_x^c} \frac{\partial^d}{\partial \phi_y^d} \mathbb{E}[\tilde{\beta}_j(x) \tilde{\beta}_{j,p}(y)] \leq B^{j(a+b+c+d)} \frac{K_M}{(1 + j^{-1} B^j d(x, y))^{4p+2-\gamma}}.$$

□

From Proposition B.1 it immediately follows that

**Lemma B.2** *There exists a constant  $K_M > 0$  such that, for all  $x, y \in \mathbb{S}^2$  we have*

$$\begin{aligned} \rho_j(\phi) &\leq \frac{K_M}{(1 + j^{-1}B^j\phi)^M}, \\ \epsilon_j(\phi), \delta_j(\phi), \alpha_{1,j}(\phi), \beta_{1,j}(\phi) &\leq B^j \frac{K_M}{(1 + j^{-1}B^j\phi)^M}, & \alpha_{2,j}(\phi), \beta_{2,j}(\phi), \gamma_{1,j}(\phi) &\leq B^{2j} \frac{K_M}{(1 + j^{-1}B^j\phi)^M}, \\ \beta_{3,j}(\phi), \gamma_{2,j}(\phi), \gamma_{3,j}(\phi) &\leq B^{3j} \frac{K_M}{(1 + j^{-1}B^j\phi)^M}, & \gamma_{4,j}(\phi) &\leq B^{4j} \frac{K_M}{(1 + j^{-1}B^j\phi)^M}. \end{aligned}$$

## References

- [1] Adler, R. J. and Taylor, J. E. (2007), *Random Fields and Geometry*, Springer.
- [2] Argueso, F., Salerno, E., Herranz, D., Sanz, J. L., Kuruoglu, E. E., Kayabol, K. (2011), A Bayesian technique for the detection of point sources in CMB maps, *Monthly Notices of the Royal Astronomical Society*, Volume 414, Issue 1, pp. 410-417, arXiv:1101.1456
- [3] Axelsson, M., Ihle, H.T., Scodeller, S., Hansen, F. K. (2015), Testing for foreground residuals in the Planck foreground cleaned maps: A new method for designing confidence masks, *Astronomy and Astrophysics*, 578, A44, arXiv:1410.7102
- [4] Baldi, P., Kerkyacharian, G., Marinucci, D. and Picard, D. (2009), Asymptotics for Spherical Needlets, *Annals of Statistics*, Vol. 37, No. 3, 1150-1171
- [5] Baldi, P., Kerkyacharian, G., Marinucci, D., and Picard, D. (2009), Subsampling needlet coefficients on the sphere, *Bernoulli* 15, 2, 438–463.
- [6] Benjamini, Y., Hochberg, Y. (1995), Controlling the false discovery rate: a practical and powerful approach to multiple testing, *J. Roy. Statist. Soc. Ser. B*, Vol. 57, no. 1, 289–300.
- [7] Bobin, J., Sureau, F., Starck, J.-L., Rassat, A., Paykari, P. (2014), Joint Planck and WMAP CMB Map Reconstruction, *Astronomy and Astrophysics*, Volume 563, id.A105, 17 pp., arXiv:1401.6016
- [8] Cammarota, V., Marinucci, D., Wigman, I. (2015), On the distribution of the critical values of random spherical harmonics, *Journal of Geometric Analysis*, arXiv:1409.1364.
- [9] Cheng, D., and Schwartzman, A. (2015), Distribution of the height of local maxima of Gaussian random fields. *Extremes*, Vol. 18, 213–240.
- [10] Cheng, D. and Schwartzman, A. (2014), Multiple testing of local maxima for detection of peaks in random fields. *Annals of Statistics*, accepted. arXiv:1405.1400
- [11] Cheng, D., Schwartzman, A. (2015), On the Explicit Height Distribution and Expected Number of Local Maxima of Isotropic Gaussian Random Fields, arXiv:1503.01328

- [12] Delabrouille, J. et. al. (2013), The pre-launch Planck Sky Model: a model of sky emission at submillimetre to centimetre wavelengths, *Astronomy and Astrophysics*, Vol.553, A96.
- [13] Dodelson, S. (2003), *Modern Cosmology*, Academic Press.
- [14] Durastanti, C. (2013), Tail Behaviour of Mexican Needlets, arXiv 1307.4553
- [15] Durrer, R. (2008), *The Cosmic Microwave Background*, Cambridge University Press.
- [16] Geller, D. and Mayeli, A. (2009), Continuous Wavelets on Compact Manifolds, *Math. Z.*, Vol. 262, pp. 895-927, arXiv: 0811.4440
- [17] Geller, D. and Mayeli, A. (2009), Nearly Tight Frames and Space-Frequency Analysis on Compact Manifolds, *Math. Z.*, Vol, 263, pp. 235-264, arXiv: 0706.3642
- [18] Geller, D. and Mayeli, A. (2009), Besov Spaces and Frames on Compact Manifolds, *Indiana Univ. Math. J.*, Vol. 58, pp. 2003-2042, arXiv:0709.2452.
- [19] Górski, K.M., Hivon, E., Banday, A.J., Wandelt, B.D., Hansen, F.K., Reinecke, M., Bartelmann, M. (2005), HEALPix: A Framework for High-Resolution Discretization and Fast Analysis of Data Distributed on the Sphere, *Astrophysical Journal*, Vol.699, pp. 759-771.
- [20] Kato, T. (1995), *Perturbation theory for linear operators*, Classics in Mathematics. Springer-Verlag, Berlin.
- [21] Lan, X., Marinucci, D. (2009), On the dependence structure of wavelet coefficients for spherical random fields, *Stochastic Process. Appl.* 119, no. 10, 3749–3766.
- [22] Leonenko, N. (1999), *Limit Theorems for Random Fields with Singular Spectrum*, Mathematics and its Applications, 465. Kluwer Academic Publishers, Dordrecht
- [23] Loh, W.-L. (2005), Fixed-Domain Asymptotics for a Subclass of Matérn-type Gaussian Random Fields, *Annals of Statistics*, Vol. 33, No. 5, 2344-2394
- [24] Loh, W.-L. (2015), Estimating the smoothness of a Gaussian random field from irregularly spaced data via higher-order quadratic variations, *Annals of Statistics*, Vol.43, no. 6, 2766-2794
- [25] López-Caniego, M., Herranz, D., Sanz, J. L., and Barreiro, R. B. (2005), Detection of Point Sources on Two-Dimensional Images Based on Peaks, *EURASIP Journal on Applied Signal Processing*, Vol. 2005, No. 15, 2426-2436, astro-ph/0503149
- [26] Marinucci, D., and Peccati, G. (2011), *Random Fields on the Sphere. Representation, Limit Theorem and Cosmological Applications*, Cambridge University Press

- [27] Marinucci, D., and Peccati, G. (2013), Mean Square Continuity on Homogeneous Spaces of Compact Groups, *Electronic Communications in Probability*, Vol. 18, n.37, 10 pp., arXiv:1210.7676.
- [28] Marinucci, D., Pietrobon, D., Balbi, A., Baldi, P., Cabella, P., Kerkyacharian, G., Natoli, P. Picard, D., Vittorio, N., (2008), Spherical Needlets for CMB Data Analysis, *Monthly Notices of the Royal Astronomical Society*, Volume 383, Issue 2, pp. 539-545
- [29] Marinucci, D., and Wigman, I. (2014), On Nonlinear Functionals of Random Spherical Eigenfunctions, *Communications in Mathematical Physics*, 327, n.3, 849-872, arXiv: 1209.1841.
- [30] Mayeli, A. (2010), Asymptotic Uncorrelation for Mexican Needlets, *Journal of Mathematical Analysis and its Applications* Vol. 363, Issue 1, pp. 336-344, arXiv: 0806.3009
- [31] Narcowich, F. J., Petrushev, P., and Ward, J.D. (2006a), Localized Tight Frames on Spheres, *SIAM Journal of Mathematical Analysis* Vol. 38, pp. 574–594
- [32] Narcowich, F. J., Petrushev, P., and Ward, J.D. (2006b), Decomposition of Besov and Triebel-Lizorkin Spaces on the Sphere, *Journal of Functional Analysis*, Vol. 238, 2, 530–564
- [33] Planck Collaboration (2014) Planck 2013 results. I. Overview of products and scientific results, *Astronomy and Astrophysics*, Volume 571, idA1, arXiv:1303.5062
- [34] Planck Collaboration (2014) Planck 2013 Results. XXIV. Constraints on Primordial non-Gaussianity, *Astronomy and Astrophysics*, Volume 571, idA24, 58 pp., arXiv:1303.5084
- [35] Planck Collaboration (2014) Planck 2013 Results. XXII. Isotropy and Statistics of the CMB, *Astronomy and Astrophysics*, Volume 571, idA23., arXiv:1303.5083
- [36] Planck Collaboration (2015) Planck 2015 results. XI. CMB power spectra, likelihoods, and robustness of parameters, <http://xxx.lanl.gov/abs/1507.02704>
- [37] Planck Collaboration (2015) Planck 2015. XXVI, The second Planck catalogue of compact sources, <http://xxx.lanl.gov/abs/1507.02058>
- [38] Rudjord, O., Hansen, F.K., Lan, X., Liguori, M. Marinucci, D., Matarrese, S. (2009), An Estimate of the Primordial Non-Gaussianity Parameter  $f_{NL}$  Using the Needlet Bispectrum from WMAP, *Astrophysical Journal*, Volume 701, Issue 1, pp. 369-376, arXiv:0901.3154
- [39] Rudjord, O., Hansen, F.K., Lan, X., Liguori, M. Marinucci, D., Matarrese, S. (2010), Directional Variations of the Non-Gaussianity Parameter  $f_{NL}$ , *Astrophysical Journal*, Volume 708, Issue 2, pp. 1321-1325, arXiv: 0906.3232

- [40] Scodeller, S., Rudjord, O. Hansen, F.K., Marinucci, D., Geller, D. and Mayeli, A. (2011), Introducing Mexican needlets for CMB analysis: Issues for practical applications and comparison with standard needlets, *Astrophysical Journal*, 733, 121
- [41] Scodeller, S., Hansen, F.K., Marinucci, D. (2012), Detection of new point sources in WMAP 7 year data using internal templates and needlets, *Astrophysical Journal*, 753, 27, arXiv:1201.5852
- [42] Scodeller, S., Hansen, F.K. (2012), Masking versus removing point sources in CMB data: the source corrected WMAP power spectrum from new extended catalogue, *Astrophysical Journal*, 761, 119, arXiv:1207.2315
- [43] Schwartzman, A., Gavrilov, Y., and Adler, R. J. (2011), Multiple testing of local maxima for detection of peaks in 1D, *Annals of Statistics*, 39, 3290–3319.
- [44] Wigman, I. (2009), On the Distribution of the Nodal Sets of Random Spherical Harmonics. *Journal of Mathematical Physics* 50, no. 1, 013521, 44 pp.
- [45] Wigman, I. (2010), Fluctuation of the Nodal Length of Random Spherical Harmonics, *Communications in Mathematical Physics*, Volume 298, n. 3, 787-831

Dan Cheng and Armin Schwartzman

Division of Biostatistics, University of California, San Diego

dcheng2@ncsu.edu; armins@ucsd.edu

Valentina Cammarota, Yabebal Fantaye and Domenico Marinucci

Department of Mathematics, University of Rome Tor Vergata

cammarot@mat.uniroma2.it; fantaye@mat.uniroma2.it; marinucc@mat.uniroma2.it